

Tropospheric Ozone trends and drivers at a Southern Hemisphere background site in Chile

Laura Gallardo^{1,2}, Charlie Opazo^{1,2}, Camilo Menares^{1,2}, Kevin Basoa^{1,3}, Lucas Castillo^{1,2}, Nikos Daskalakis⁴, Maria Kanakidou^{4,5,6}, Carmen Vega⁷, Nicolás Huneus^{1,2}, Roberto Rondanelli^{1,2} and Rodrigo Seguel^{1,2*}

¹ Center for Climate and Resilience Research (CR2, FONDAP 15110009), Santiago, Chile

² Departamento de Geofísica, Facultad de Ciencias Físicas y Matemáticas, Universidad de Chile, Santiago, Chile

³ Ministry of the Environment, Chile

⁴ Laboratory for Modeling and Observation of the Earth System (LAMOS), Institute of Environmental Physics (IUP), University of Bremen, Bremen, Germany

⁵ Environmental Chemical Processes Laboratory, Department of Chemistry, University of Crete, Heraklion, Greece

⁶ Center for the Study of Air Quality and Climate Change, Foundation for Research and Technology – Hellas, Patras, Greece

⁷ ~~Dirección Meteorológica de Chile~~, Dirección de Aeronáutica Civil de Chile

*Now at Faculty of Chemistry, Pontifical Catholic University, Chile.

Correspondence to: Laura Gallardo (lgallard@u.uchile.cl)

Abstract

Tropospheric ozone (O₃) is a significant anthropogenic climate forcer with uncertain distribution in the Southern Hemisphere due to sparse observations. This study analyzes 28 years of in situ ozone, methane, carbon monoxide, and meteorological data at Tololo (30.17° S, 70.80° W, 2154 m a.s.l.), Chile, integrating reanalysis and atmospheric chemistry modeling. Here we identify a rising ozone trend of 2.1±0.8 ppbv per decade since 2006, ~~primarily possibly~~ driven by increasing background methane. We quantify contributions from biomass burning and transport of stratospheric and upper tropospheric air to Tololo~~stratosphere to troposphere transport~~, each adding approximately 5 ppbv per event during late winter and spring O₃ maximum. ~~Stratospheric Events of air of stratospheric and upper tropospheric origin intrusions~~ are linked to synoptic-scale troughs and cutoff lows, modulated by El Niño Southern Oscillation phases. These findings enhance understanding of ozone variability in the Southern Hemisphere free troposphere and underscore the importance of sustained observations at Tololo to monitor tropospheric ozone dynamics amid climate change.

1. Introduction

Tropospheric ozone (O₃) is the third largest anthropogenic climate forcer (Checa-Garcia et al., 2018; Forster et al., 2021; Myhre et al., 2013; Skeie et al., 2020). It also affects the terrestrial carbon sink by altering photosynthesis (Fu et al., 2020; Kumar Mishra et al., 2024). Further, it is central to the cleansing capacity of the atmosphere as it is an oxidant and the

1 precursor of the hydroxyl radical (OH) (Murray et al., 2014; Thompson, 1992), which in turn determines the lifetime of the
2 second largest anthropogenic climate forcer, i.e., methane (He et al., 2020; Young et al., 2013). Also, tropospheric ozone can
3 adversely affect human health (Fleming et al., 2018; Nuvolone et al., 2018) and vegetation (Ainsworth, 2017; Mills et al.,
4 2016). On the other hand, oxidants, including O₃, mediate the formation of secondary particles that are key to air quality and
5 radiative balance, particularly at the regional scale (Karset et al., 2018; Turnock et al., 2020).

6 In the remote troposphere, ozone (O₃) is primarily produced through the oxidation of long-lived species such as
7 methane (CH₄), carbon monoxide (CO), and secondary oxygenated compounds, provided that sufficient nitrogen oxides (NO_x
8 = NO + NO₂) are present (Crutzen, 1988; Crutzen et al., 1999). In contrast, in more polluted regions, O₃ formation is dominated
9 by the oxidation of short-lived volatile organic compounds (VOCs) (Archibald et al., 2020; Monks et al., 2015). In the absence
10 of NO_xnitrogen oxides, different oxidation pathways are favored that lead to the destruction of ozone. The second largest
11 contribution to the tropospheric ozone budget is stratosphere-to-troposphere transport (STT) (Archibald et al., 2020; Young et
12 al., 2018). Near the surface, O₃ is removed from the atmosphere by dry deposition (Clifton et al., 2020). All these processes,
13 and particularly photochemical production and destruction, result in a highly non-linear behavior that is sensitive to changes
14 in precursors — e.g., VOCs and nitrogen oxides— and climate variability and change (Barnes et al., 2016; Griffiths et al., 2021;
15 Inness et al., 2015).

16 According to the sixth assessment report (AR6) of the Intergovernmental Panel on Climate Change (IPCC),
17 tropospheric ozone considering both column and free troposphere observations, has exhibited increasing trends since the mid-
18 1990s, with rates of 1 to 4 ppbv/decade in the Northern Hemisphere (NH), 1 to 5 ppbv/decade in the tropics, and less than 1
19 ppbv/decade in the Southern Hemisphere (SH) (Gulev et al, 2023). These trends are mostly influenced by changes in ozone
20 precursors—whose interactions are highly nonlinear—and possibly to a minor degree, by transport processes, particularly
21 variations in stratosphere-troposphere exchange (STE)(Li et al., 2024; Neu et al, 2014; Škerlak et al., 2014). STE changes are
22 in turn affected by chemical —e.g., ozone depleting substances— and transport —Brewer-Dobson circulation— processes in
23 the lower stratosphere in the context of global change (Akritidis et al., 2019 and references therein). Global warming is
24 projected to widen the Hadley circulation, thereby altering the location and intensity of STE (Hu et al., 2018; Lu et al., 2019).
25 Additionally, meteorological phenomena such as the El Niño Southern Oscillation (ENSO), Quasi-Biennial Oscillation (QBO),
26 and Madden-Julian Oscillation (MJO) also modulate tropospheric ozone levels (e.g., Sekiya and Sudo, 2012).

27 Observations from various platforms—including aircraft, ozone sondes, and satellites—indicate that the global
28 burden of tropospheric O₃ has increased since the second half of the 20th century (Gaudel et al., 2018; Tarasick et al, 2019;
29 Gulev et al, 2021). Until the 1980s, high ozone concentrations were observed over and downwind of North America and
30 Europe, regions where anthropogenic emissions of O₃ precursors were at their peak. Since then, these emissions have shifted
31 toward lower latitudes, resulting in elevated O₃ levels in East and South Asia (Szopa et al, 2021). Global-scale atmospheric
32 chemistry modeling studies attribute the rise in tropospheric O₃ since pre-industrial times primarily to increasing anthropogenic
33 emissions of O₃ precursors (e.g., Griffiths et al., 2021; Szopa, 2021). This increase has contributed to a global climate forcing
34 of 0.47±0.23 W/m², as reported in AR6 (Forster et al, 2021). Because the lifetime of tropospheric O₃ is relatively short (25.5

1 ± 2.2 days on average) (Griffiths et al., 2021), its distribution is spatially heterogeneous, reflecting the complex, nonlinear
2 interactions among precursors and atmospheric dynamics. The approximately 50% uncertainty in the estimate of global climate
3 forcing from tropospheric O₃ arises from two main sources: first, the lack of pre-industrial ozone observations, and second,
4 uncertainties in the current distribution of tropospheric O₃ (Szopa, 2021 and references therein). Recent advances using oxygen
5 isotopic studies (e.g., clumped isotopes, ¹⁸O¹⁸O) have helped constrain the former, suggesting a less than 40% increase in
6 tropospheric O₃ burden from preindustrial times to 2005, with most of this increase occurring between 1950 and 1980 in the
7 Northern Hemisphere- (Yeung et al., 2019). The latter source of uncertainty is due to the scarcity and uneven spatial coverage
8 of observations, especially in the upper troposphere of the tropics and subtropics, where ozone's radiative forcing is most
9 effective (Kuai et al., 2017). Global anthropogenic emissions of CO and NO_x, mainly from fossil fuel combustion, rose sharply
10 between 1950 and 1980, followed by a period of slower growth (NO_x) or decline (CO), with a noticeable shift in emission
11 hotspots toward the Equator (Hoesly et al., 2018; [Zhang et al. 2016](#); Szopa et al, 2021).

12 Methane (CH₄) is a major contributor to increased ozone in the background atmosphere ([Fiore et al. 2008](#); [West et](#)
13 [al 2007](#)). Globally averaged *in situ* observations indicate that CH₄ concentrations have risen from approximately 1630 ppbv in
14 early 1984 to 1943 ppbv in late 2024 (https://www.gml.noaa.gov/ccgg/trends_ch4/, retrieved Feb 2 2025). This increase has
15 not been uniform: there was a sharp rise between 1980 and 1990, a plateau from 1990 to the mid-2000s, and then another sharp
16 increase to the present, largely driven by anthropogenic activities (Gulev et al., 2023 [and references therein](#)). According to
17 Zhang et al. (2021), methane accounted for about 27% of the total increase in the ozone burden between 1980 and 2010. Due
18 to its relatively long atmospheric lifetime (about 9 years), methane influences global tropospheric O₃ levels regardless of its
19 emission source region. In contrast, changes in CO, VOCs, and NO_x—each with much shorter atmospheric lifetimes—result
20 in more localized and regionally differentiated impacts on ozone. Modeling studies indicate that the tropospheric O₃ burden is
21 particularly sensitive to changes in precursor emissions in tropical and subtropical regions, which have also experienced rapid
22 increases in tropospheric O₃, especially in Southeast Asia (Zhang et al., 2016, 2021).

23 Biomass burning is a significant source of O₃ precursors, including remote areas in the SH as inferred from both
24 modeling and observational studies (Bourgeois et al., 2021; Daskalakis et al., 2022). This source is particularly relevant in the
25 SH extratropics during the austral spring, where long-range transport of fire emissions from Southeast Asia, South America,
26 Southern Africa, and Oceania, affects the tropospheric O₃ column over the otherwise pristine Southeastern Pacific (Daskalakis
27 et al., 2022). Bourgeois et al. (2021) estimate the contribution of biomass burning to tropospheric O₃ to be 2 to 10 times larger
28 than that of urban (fossil fuel burning) in the SH, a contribution that is typically underestimated by global chemistry transport
29 models.

30 Cooper et al. (2020) reported surface O₃ trends at 27 globally distributed remote locations, of which only 7 were in
31 the SH. This study provided, *i.a.*, a range of regional long-term (at least 20 years) O₃ trends for the evaluation of global
32 chemistry-climate models. In the SH, most stations (5 out of 7) showed positive trends, while in the NH it was evenly split
33 between positive and negative trends. A similar result is found by Christiansen et al. (2022), who considered 13 surface stations
34 in the SH. Christiansen et al. (2022) also reports that models do not capture long-term O₃ trends throughout the troposphere

1 around the world, typically underestimating those trends (They considered 25 ozone sounding sites over the period 1990-
2 2017).

3 In summary, observations of ozone in remote regions—especially in the tropics and subtropics—are essential for
4 quantifying its variability and trends, validating atmospheric chemistry models, and accurately estimating the climate forcing
5 associated with tropospheric ozone. However, measurements in the subtropical Southern Hemisphere mid-troposphere remain
6 scarce, limiting our understanding of ozone drivers in this region. In this study, we combine 28 years of in situ measurements
7 of O₃ and meteorological variables at Tololo (30.17° S, 70.80° W, 2154 m a.s.l., Chile) with reanalysis data and measurements
8 of CO and CH₄ to assess changes in the O₃ trend. Furthermore, by employing a Generalized Additive Model (GAM) and three-
9 dimensional atmospheric chemistry simulations, we evaluate the role of background CH₄ and other factors in explaining the
10 observed increase in O₃, as well as the contributions of biomass burning and [air of stratospheric and upper tropospheric origin,](#)
11 [including](#) stratosphere-to-troposphere transport, particularly during the late winter and spring ozone maximum.

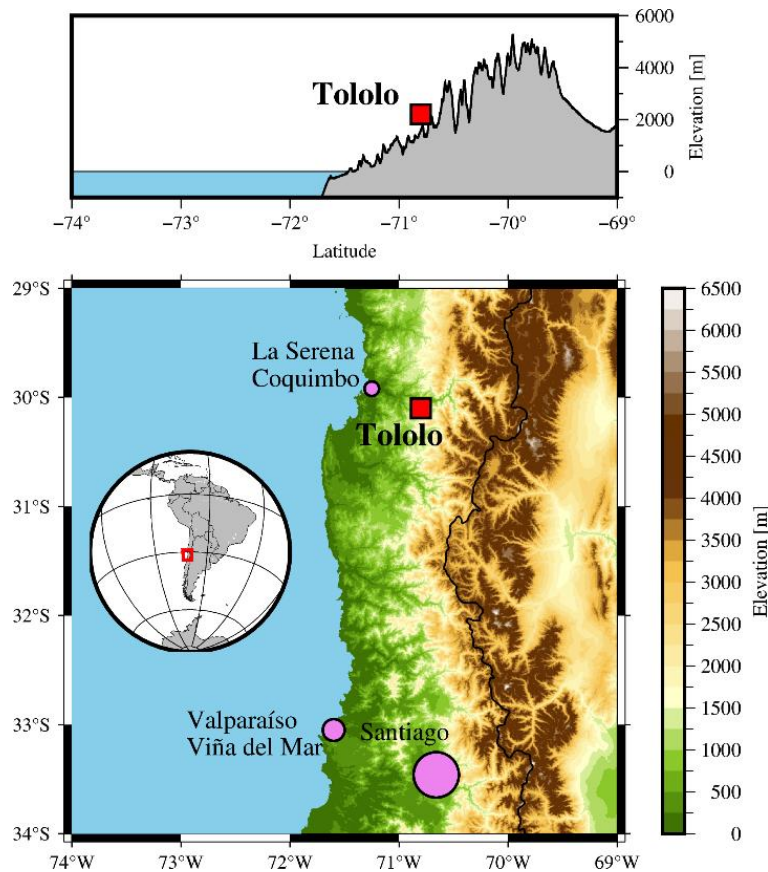
12 The paper is organized as follows. In section 2 we describe the observation site in some detail as well as the data used
13 in our study. Also, we describe the application of a Generalized Additive Model (GAM) to assert the dependence of the ozone
14 time series on methane, local and remote meteorology, seasonality, etc. Results and discussion are presented in section 3.
15 Section 4 provides a summary and conclusions of this work.

16 **2. Data and methodology**

17 **2.1 Site description**

18 The Chilean Meteorological Service (In Spanish, *Dirección Meteorológica de Chile*, DMC), under the auspices of
19 the Global Atmospheric Watch Programme (GAW) of the World Meteorological Organization (WMO), has maintained the
20 Tololo station (30.17° S, 70.80° W, 2154 m a.s.l.) in the premises of the Interamerican Southern Astronomical Observatory
21 since late 1995. The site is located about 50 km east of the Chilean coast, where the fast-growing conurbation of La Serena-
22 Coquimbo is located. Despite this urban expansion, there is no evidence of increased impact from local emissions at Tololo,
23 as discussed in later sections. Details on urban population and infrastructure in the region are provided in Figure S1 of the
24 Supplementary Material.

25 In addition to the urban areas in the surroundings of Tololo, there is a potential influence of the large urban areas to
26 the south of it: Santiago, the capital city, and the conurbation of Valparaíso-Viña del Mar (Anet et al., 2017) as illustrated in
27 Figure 1. In this case we consider whole provinces as there are smaller urban areas functionally connected to Santiago and
28 Valparaíso-Viña del Mar cities. While in 1992 the population of Santiago (Valparaíso-Viña del Mar) was 5258 k inhabitants
29 (808 k inhabitants), in 2024 it is estimated to be 8421 k inhabitants (1104 k inhabitants), corresponding to a 60% (37%)
30 percentage growth rate. We show evidence that this influence is sporadic.



1
2 **Figure 1. Location of Tololo station. The upper map shows Tololo’s location in the west of South America. The upper map**
3 **also shows Tololo’s position on a mountain top above 2000 m a.s.l along a transect at 30°S. The lower map shows the complex**
4 **topography of the area with the Andes cordillera a few kilometers east of the Tololo site. The location of three major urban areas,**
5 **i.e., the conurbations of La Serena-Coquimbo, Valparaíso-Viña del Mar and the capital city of Santiago are also shown.**

6 Over the years, this station’s topography and atmospheric circulation have been described in some detail (Anet et al.,
7 2017; Gallardo et al., 2000; Kalthoff et al., 2002; Rondanelli et al., 2002). The area surrounding Tololo is characterized by
8 highly complex topography, with deep valleys and the Andes cordillera located just 30 km east of Cerro Tololo, reaching
9 elevations up to 6 km a.s.l. Most of the time, Tololo is immersed in the free troposphere and influenced by the subsidence
10 regime of the South Pacific high, which brings clear sky conditions—a factor that has contributed to the establishment of
11 numerous astronomical observatories in the region. In winter, the subtropical jet stream (STJ) is located on average at 30°S.
12 From time to time, cutoff lows and deep troughs from higher latitudes may reach the Tololo area inducing tropopause breaks
13 and/or upward mixing of marine boundary layer air. Above 4 km a.s.l., large-scale westerly winds prevail, while northerly
14 winds are observed in a band between 2 and 4 km a.s.l., which results from the blocking effect of the westerly flow by the
15 Andes. In addition to these features, a radiatively driven circulation that is intensified in summer is present with up-slope
16 (down-slope) winds during the afternoon (night/early morning) at Tololo.

2.2 In situ measurements at Tololo

Surface O₃ has been measured in Tololo since November 1995. The technique used is UV absorption as detailed in Anet et al. (2017). This station is part of GAW, and data used here (hourly averages between November 1995 and December 2023) were downloaded from the EBAS database (<https://ebas.nilu.no/>, latest access: 1 August 2024), thus it is subject to quality standards and rigorous scrutiny.

The station was equipped with a new ozone monitor and a CO, CO₂, and CH₄ analyzer (Picarro Inc. G2401) by the Swiss Federal Laboratories for Materials Science and Technology (EMPA) in 2013. CO data are available until 2022 and CH₄ until 2023. Data were downloaded from <https://gaw.kishou.go.jp/>, latest access: 1 August 2024. Calibration procedures are detailed in the metadata.

Standard meteorological data –wind, temperature, pressure and solar radiation– are also measured at the station. The data for the period between 1995 and 2023 were retrieved from the data base of the Chilean Weather Service (<https://climatologia.meteochile.gob.cl/application/informacion/fichaDeEstacion/300034>, last access: 1 October 2024). As explained later, these data were used to correct the reanalysis data at 775 hPa. We did not use the observed data because there were significant data gaps, particularly regarding humidity.

2.3 Reanalysis and large-scale variability data

We used ERA5 data (Hersbach et al., 2020) instead of the local time series for temperature, humidity, and winds, extracting values at 30.25°S, 70.75°W and 775 hPa, the grid point closest to Tololo's actual location. A bias was identified in the ERA5 time series when compared to available in situ measurements (see Figure S2). To correct ~~for~~ this, we applied a Quantile Delta Mapping bias correction to the ERA5 data for Tololo. The correction was performed separately for each month and hour: for example, to adjust values at 00:00 in January, all observational and ERA5 data for January at that hour, as well as data from two hours before and after (a 5-hour window), were used to calculate the adjustment, which was then applied to the January 00:00 data. This procedure was repeated for each hour and month, resulting in a specific correction for every month-hour combination.

We also used ERA5 data to identify synoptic conditions consistent with stratospheric intrusions or downward transport of upper tropospheric air. To this end, we utilized geopotential height and vertical velocity at 500 hPa to estimate horizontal anomaly composites, as well as potential vorticity and specific humidity between 900 and 200 hPa to estimate a vertical cross section (longitude-pressure) along 30.25°S. To calculate anomalies, firstly we estimated the climatological annual cycle between 1995-2023 based on daily data. Thereafter we applied a Fourier filter to eliminate high frequency fluctuations (sub seasonal). Then, we calculated the anomaly as the difference between the 24-hour running mean of the time series and the smoothed climatology.

To assess how climate variability affects long-term trends at Tololo, we considered ENSO, QBO and MJO in our GAM analysis described later. For El Niño-La Niña we used the Multivariate ENSO Index version 2 (MEI). It corresponds to

1 the bi-monthly mean of the principal component of the combined empirical orthogonal function of five observed variables
2 over the tropical Pacific: sea level pressure, surface temperature, surface zonal wind, surface meridional wind, and outgoing
3 longwave radiation. This index is ~~elaborated~~ provided by NOAA Physical Sciences Laboratory
4 (<https://www.psl.noaa.gov/enso/mei>, last access: 30 March 2024).

5 For QBO, we used the monthly mean zonal wind measured by meteorological soundings in Singapore (01.22N,
6 103.55E) in 50 (QBO50) and 30 (QBO30) hPa. Monthly means are calculated from daily data in Singapore. Data were obtained
7 from the National Aeronautics and Space Administration (NASA), at the Goddard Space Flight Center (GSFC) (https://acd-ext.gsfc.nasa.gov/Data_services/met/qbo/QBO_Singapore_Uvals_GSFC.txt, last access: 25 October 2024).

8 In the case of MJO, we used the Real-Time Multivariate (RMM) MJO daily index (Gottschalck et al., 2010; Wheeler
9 & Hendon, 2004). It corresponds to the first two principal components of the combined empirical orthogonal functions between
10 15°N-15°S of anomalous 200 and 850-hPa zonal winds and outgoing longwave radiation. It was retrieved from the Bureau of
11 Meteorology Australia (<http://www.bom.gov.au/climate/mjo/>, last access: 29 May 2024).

13 2.4 Other ancillary data

14 As indicated before, CH₄ has been recorded at Tololo for the period 2013-2023. To complete the time series to the
15 period before 2013, we used data collected at Rapa Nui (Easter Island, 27.8S, 109.8W, 51m a.s.l.), which is an ozone sounding
16 monitoring station under GAW (Gallardo et al., 2016). In addition to ozone soundings, the National Oceanic and Atmospheric
17 Administration (NOAA, <https://gml.noaa.gov/dv/site/?stacode=EIC>) maintained, *i.a.*, weekly CH₄ flask measurements on the
18 island between 1994 and 2019. Firstly, we compared both time series over the period 2013-2019, and we found slightly higher
19 values at Tololo (See methane at Rapa Nui and Tololo in Figure S 3). As the differences in methane between both sites were
20 deemed minor – possibly due to oceanic upwelling near Tololo (Weber et al., 2019)– and given the long turn-over time of
21 CH₄, we decided to extend Rapa Nui CH₄ by means of a simple linear regression of simultaneous measurements. We took
22 Tololo measurements at 22 UTC on the same days as they are available at Rapa Nui. Once the regression had been performed,
23 we used it to extend the CH₄ time series for Rapa Nui until 2023 and used them for Tololo. These data were then used in our
24 GAM to assess the influence of methane on the long-term trend of ozone measured at Tololo. Lastly, we estimated a smooth
25 time series (with annual seasonality) and a smooth trend (without seasonality) to represent the new time series for CH₄
26 according to (Thoning et al., 1989). We used the code available at NOAA (<https://gml.noaa.gov/aftp/user/thoning/ccgerv/>, last
27 access 15 October 2024).

28 2.5 Identifying the influence of biomass burning

29 We use outputs from a global atmospheric chemistry model to estimate the contribution of biomass burning at Tololo.
30 The model is TM4-ECPL as described in Daskalakis et al. (2022). The model has a horizontal resolution of 3° longitude×2°
31 latitude, with 34 hybrid vertical layers up to 10 hPa. We use assimilated meteorology from ERA interim. The model was run
32 over the period ~~1995-1980 to 2015, and we use the period 1995-and~~ 2015. Differently from Daskalakis et al. (2022) the model

1 has been re-run using updated emissions as used in AR6, i.e., emissions as described in Hoesly et al. (2018) and Van Marle
2 et al. (2017). The model was run with and without biomass burning to estimate the contribution of this source of precursors to
3 ozone.

4 Despite its resolution, the model captures the seasonal and, partly the day-to-day, possibly synoptical in origin,
5 variability as inferred from the comparison with daily mean observations of CO. However, there is a positive model bias (~7
6 ppbv), and a larger distance between model and observations of CO in the upper tail of the data distribution (See Figure S 4).
7 Hence, we performed a bias correction of the model data. To do so, we followed a similar approach to that used for ERA 5
8 data, and as also applied by Staehle et al. (2024) and implemented by Schwertfeger et al. (2023). Thereafter, we applied the
9 bias correction to the rest of the model data set. We assumed that the adjusted model CO kept the same ratio with biomass
10 burning CO as the original data, which allowed us to also adjust the biomass signal. The characterization regarding the
11 influence of biomass burning is restricted to the period between 1995 and 2015 for which we have TM4-ECPL data.

12 2.6 Identifying air of stratospheric or upper tropospheric origin intrusions

13 Air of Stratospheric or upper tropospheric origin, hereafter SUTO, intrusions are is characterized by relatively high
14 O₃ and low water vapor mixing ratios, thus we used the hourly time series of O₃ and specific humidity at Tololo to identify
15 SUTO events stratospheric intrusions. Firstly, we calculated enhancements of O₃ over a 10-day running mean of O₃ and a
16 simultaneous reduction in specific humidity over a 10-day period similarly to Cui et al. (2009). Differently from Cui et al.
17 (2009), we also averaged specific humidity and did not use relative humidity but specific humidity. After ~~a careful~~careful
18 visual inspection of the data, we defined ~~the arrival of SUTO a stratospheric intrusion event~~ as a continuous period where
19 simultaneously hourly O₃ was 10% above the 10-day running average, and ~~hourly 24 running average of~~ specific humidity
20 was less than ~~70~~15% of the 10-day running mean. The minimum duration of an event was set to be ~~12-18~~ hours ~~or half a day~~
21 to ~~account exclude for~~ fast passing synoptic and sub synoptic perturbations. To avoid identification problems due to missing
22 data, high frequency variability or errors associated with using specific humidity from ERA5, we ~~slightly~~ relaxed the continuity
23 criterion. ~~Once an event was identified, We allowed~~we allowed up to a maximum of ~~6-18~~ hours after the event in which the
24 above criteria might not be met in all hours and still be considered part of the same ~~event, reducing the total number of those.~~
25 ~~We recognize that~~ While many criteria may be established to identify SUTO and that the chosen thresholds are somewhat
26 arbitrary, quantify the intensity of an event, we opted to consider the duration of the event as the intensity indicator. Also, as
27 TM4-ECPL has a dedicated stratospheric ozone tracer that was used to estimate the ozone of stratospheric origin arriving in
28 Tololo, we were able to get an independent estimate. ~~We compared the results from the of the stratospheric contribution to~~
29 ozone at Tololo empirical method indicated above with the model outputs.

30 2.7 Estimating trends

31 The term trend is not uniquely defined in statistics (Capparelli et al., 2013), and calculated trends are method
32 dependent (Franzke, 2012). There are multiple statistical approaches to estimating trends in time series and they must be

1 carefully chosen and interpreted (Chang et al., 2021, 2023; Cooper et al., 2014, 2020; Gaudel et al., 2018), particularly when
2 dealing with nonlinear and nonstationary data, with marked seasonality and interannual and decadal variability such as surface
3 ozone at Tololo. As the climate system is complex, many processes interact with each other at multiple temporal and spatial
4 scales leading to nonlinear responses to external and internal changes (Snyder et al., 2011; Wang et al., 2023). Intrinsic climate
5 variability plays an important role when assessing trends at the local and regional scales (Franzke, 2012). According to the
6 same author, intrinsic climate variability leads to a so-called “stochastic trend” as it is expressed in autocorrelation (variables
7 show temporal correlation), whereas a so-called “deterministic trend” emerges due to an external forcing. In general, detecting
8 trends depends upon the size of the trend, the time span of available data, and the magnitude of variability and autocorrelation
9 of the noise in the data (Weatherhead et al., 1998). In the case of atmospheric chemistry variables, one must add uncertainties
10 derived from instrument detection level and sampling, change of sensors, the influence of extreme events, etc. (Chang et al.,
11 2021).

12 The Tropospheric Ozone Assessment Report (TOAR) initiative has made a substantial contribution to standardizing
13 the methods to visualize and calculate trends for data as those collected at Tololo. Hence, we use the Quantile Regression
14 algorithm that allows piecewise detection of change points by Chang et al. (2023). Again, the concept of change point is not
15 well-defined in statistics, nonetheless it is a useful indicator of significant changes in a time series over time, for instance
16 change of instruments. In the case of Tololo, the ozone sensor was replaced in 2013 (Anet et al., 2017). We will assess whether
17 this change is apparent in the data.

18 **2.8 Generalized Additive Models for Tololo**

19 Generalized Additive Models (GAMs) are an extension of linear models, allowing nonlinear and nonparametric
20 fittings of complex dependences of response variables on explanatory variables. A GAM adopts a sum of arbitrary functions
21 of variables —potentially nonlinear— that represent different features via splines, which altogether describe the magnitude
22 and variability of the response variables (Hastie and Tibshirani, 1986; Molnar, 2025). The choice of explanatory variables is
23 key. It must be based on physical reasoning about potential contribution of variables that one can logically expect to explain
24 the response variable. Statistically, one should choose variables that contribute to explaining the response variable but are
25 largely independent from one another (Kovács, 2024). Redundancy results in unstable parameter estimates in GAMs and
26 makes the marginal effect of features harder to interpret. In the case of atmospheric variables, one cannot assure orthogonality
27 among explanatory variables as they are generally autocorrelated, but an effort must be made to avoid redundancy. In this
28 study, we applied expert knowledge, and partial dependence plots (Hastie et al., 2009) to assess the physical meaning and
29 functional dependences of the estimated relationships and thereby interpreting the GAM results. Additionally, we used the
30 SHapley Additive exPlanations (SHAP) approach –based on game theory– to determine the ranked contribution of each
31 explanatory variable in GAM (Lipovetsky and Conklin, 2001). In a simplified manner, a GAM is of the form (Eq.1):

$$32 \quad O_3 = \epsilon + f_1(v_1) + f_2(v_2) + \dots + f_N(v_N) \text{ (Eq. 1)}$$

1 where ϵ represents an error term, and f_i , $i=1, N$ are spline functions of variables v_i , $i=1, N$ such as specific humidity,
2 temperature, wind speed, etc. (Hastie and Tibshirani, 1986; Molnar, 2025). The error term has a stochastic component, so we
3 run our GAM 50 times. We utilized the following Python software: pyGAM available <https://pygam.readthedocs.io/en/latest/>
4 and shap available at <https://shap.readthedocs.io/en/latest/>.

5 **3. Results and discussion**

6 **3.1 Change points and trend estimates**

7 Seguel et al. (2024) analyze the ozone time series at Tololo over the period (1995-2021). They identify two change
8 points in ozone, one in early 2006 and another in early 2014, both within uncertainties of several years. As the authors note,
9 the 2006 change point coincides with the global increase in methane, also observed at Rapa Nui (Easter Island). In this work,
10 we extend the analysis to include 2022 and 2023 and explore the role of several atmospheric variables. Thus, we repeat the
11 change point analysis for ozone as well as for methane, temperature (T), specific humidity (q), dewpoint temperature (T_d), and
12 geopotential height at 500 hPa (Z_{500}).

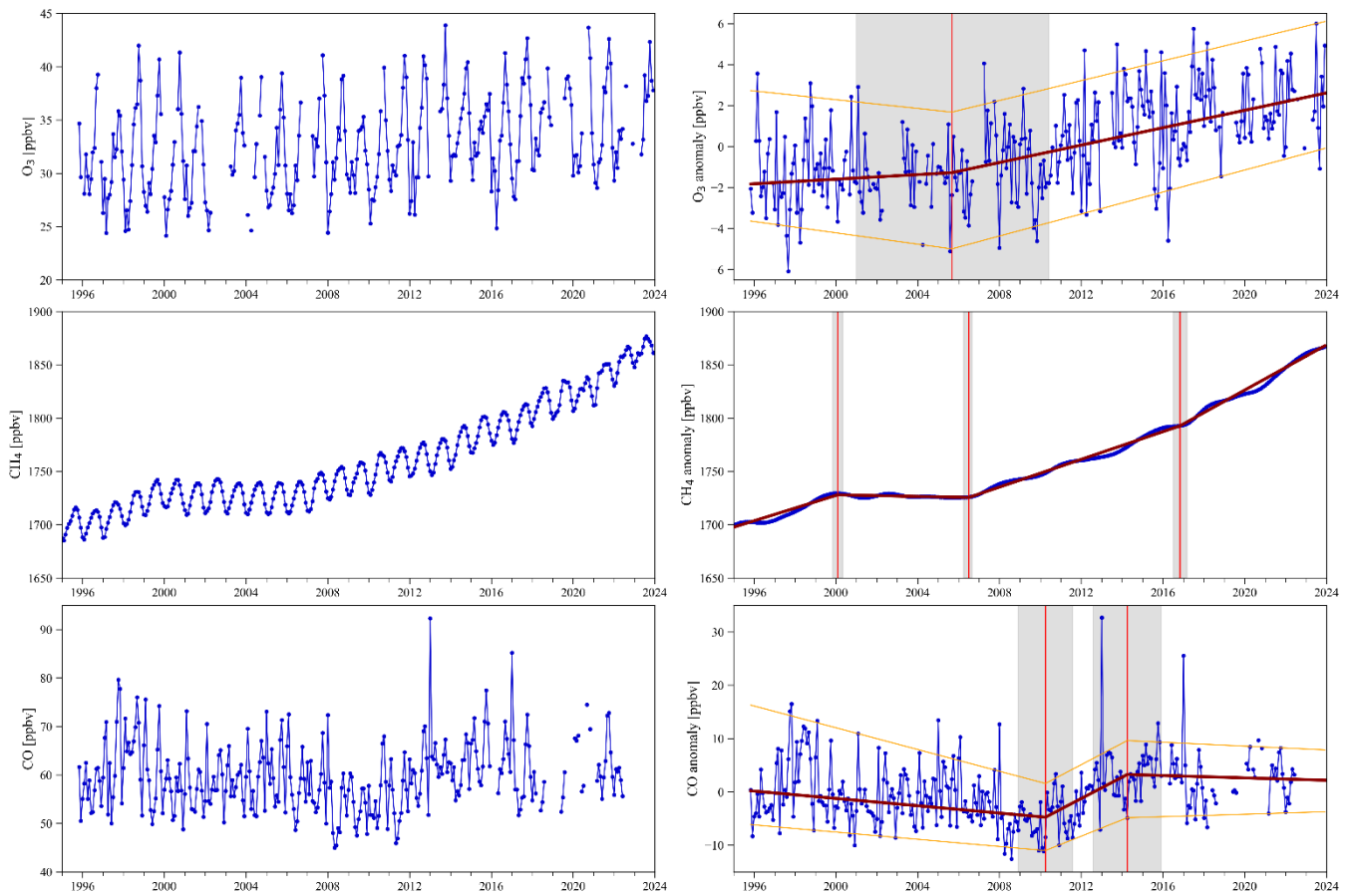
13 Methane was chosen due to its role as O_3 precursor in the background atmosphere (Crutzen, 1988; Crutzen et al.,
14 1999). We included T because, in addition to typically explaining a significant part of the variance of near surface O_3 , key
15 reactions leading to O_3 production depend on temperature (Pusede et al., 2015). Specific humidity was selected since the
16 principal global sink of tropospheric O_3 is the photolysis by near ultraviolet radiation ($\lambda < 310$ nm) in the presence of water
17 vapor (Jacob and Winner, 2009). We chose specific humidity instead of relative humidity to separate the effect of temperature
18 from that of humidity. Dewpoint has been used as a meteorological explaining factor at Mauna Loa, allowing the separation
19 between dry air associated with higher altitude and latitude air masses, and moist conditions associated with more tropical air
20 masses, when applied to nighttime values avoiding upslope data (Gaudel et al., 2018). At Tololo, higher latitude air masses
21 can be moist as they reach this subtropical site ($30^\circ S$) in connection with deep troughs and cutoff lows (Fuenzalida et al., 2005;
22 Rondanelli et al., 2002), while subtropical air masses are typically dry. Geopotential height at 500 hPa is used as an indicator
23 of synoptic scale variability. These times series and their change points are illustrated in Figures 2 and 3.

24 Figure 2 shows the strong seasonality in O_3 , CH_4 and CO. In addition to a marked seasonality, the most prominent
25 characteristic of ozone is the maximum values that are observed in spring (Anet et al., 2017; Gallardo et al., 2000). Carbon
26 monoxide also peaks in spring, except for some summer events. This maximum in ozone and CO is generally attributed to
27 biomass burning (Anet et al., 2017; Daskalakis et al., 2022). But as we will see later, many SUTO events occur in connection
28 with synoptic conditions consistent with STE, which may also plays a role in late winter and spring for ozone (Daskalakis et
29 al., 2022; Rondanelli et al., 2002). The variability in methane, on the other hand, is less marked with a February-March
30 minimum, and an August-September maximum, which is largely driven by the hydroxyl radical sink (East et al., 2024). ENSO
31 also plays a role in methane interannual variability (Rowlinson et al., 2019), which will affect its seasonal variation too. The

1 influence of ENSO, QBO, MJO has been found to be relevant for the variability of tropospheric ozone and its precursors
2 (Daskalakis et al., 2022 and references therein).

3 Except for methane, change points calculated for all species are subject to multi-year uncertainties, which is to be
4 expected given the relatively large variability of the time series (Muggeo, 2017), including long-term modes of variability
5 (e.g., Pacific Decadal Oscillation, PDO) that may not be captured by the relatively short times series. The change point for
6 ozone is estimated to occur near August 2005 with an uncertainty range between 2001 and mid-2010, which largely coincides
7 with the upward acceleration of methane growth by mid-2006. The addition of the years 2022 and 2023 resulted in a sole
8 change point near 2006, instead of two as shown by Seguel et al. (2024). Interestingly, ozone shows a growing positive median
9 trend of the ~~median trend~~ both before and after 2006, the rate of growth being larger after 2006 than before 2006. The near
10 2006 change in ozone coincides with a marked increase in the rate of change in methane, which is suggestive but difficult to
11 reconcile with the long turnover time of methane, and the absence of enough NO_x in the region of interest, except perhaps in
12 connection with long-range transport of biomass burning, is physically reasonable (methane) and consistent with the visual
13 inspection of the time series. There is no evidence of an effect of the change of instruments in 2013. Interestingly, ozone shows
14 a growing median trend both before and after 2006, the rate of growth being larger after 2006 than before 2006. The 5th and
15 95th percentiles of O₃ indicate decreasing trends before 2006 and growing trends thereafter suggesting a more significant
16 influence of extreme events in the later period such as summer wildfires along central and Southern Chile or during the CO₂
17 Virus Disease pandemic (Seguel et al., 2024). Over the period 2006-2023, ozone (median) shows a trend of about 2.1
18 ppbv/decade. Thus, over 17 years, the corresponding change in ozone is ca. 3.6 ppbv. Assuming this is well mixed, the
19 corresponding change in ozone mass burden is 30 TgO₃ or a yearly average of 1.8 TgO₃. Over the same period methane volume
20 mixing ratios have changed by 145 ppbv, which corresponds to a change in mass burden of 408 TgCH₄. Thus, the mass burden
21 ratio between ozone and methane is ≈ 0.08 TgO₃/ TgCH₄, which is in lower end but consistent with previous global model
22 estimates, i.e., a range between 0.12 and 0.16 (Fiore et al, 2008) and 0.09 to 0.19 (West et al, 2007).

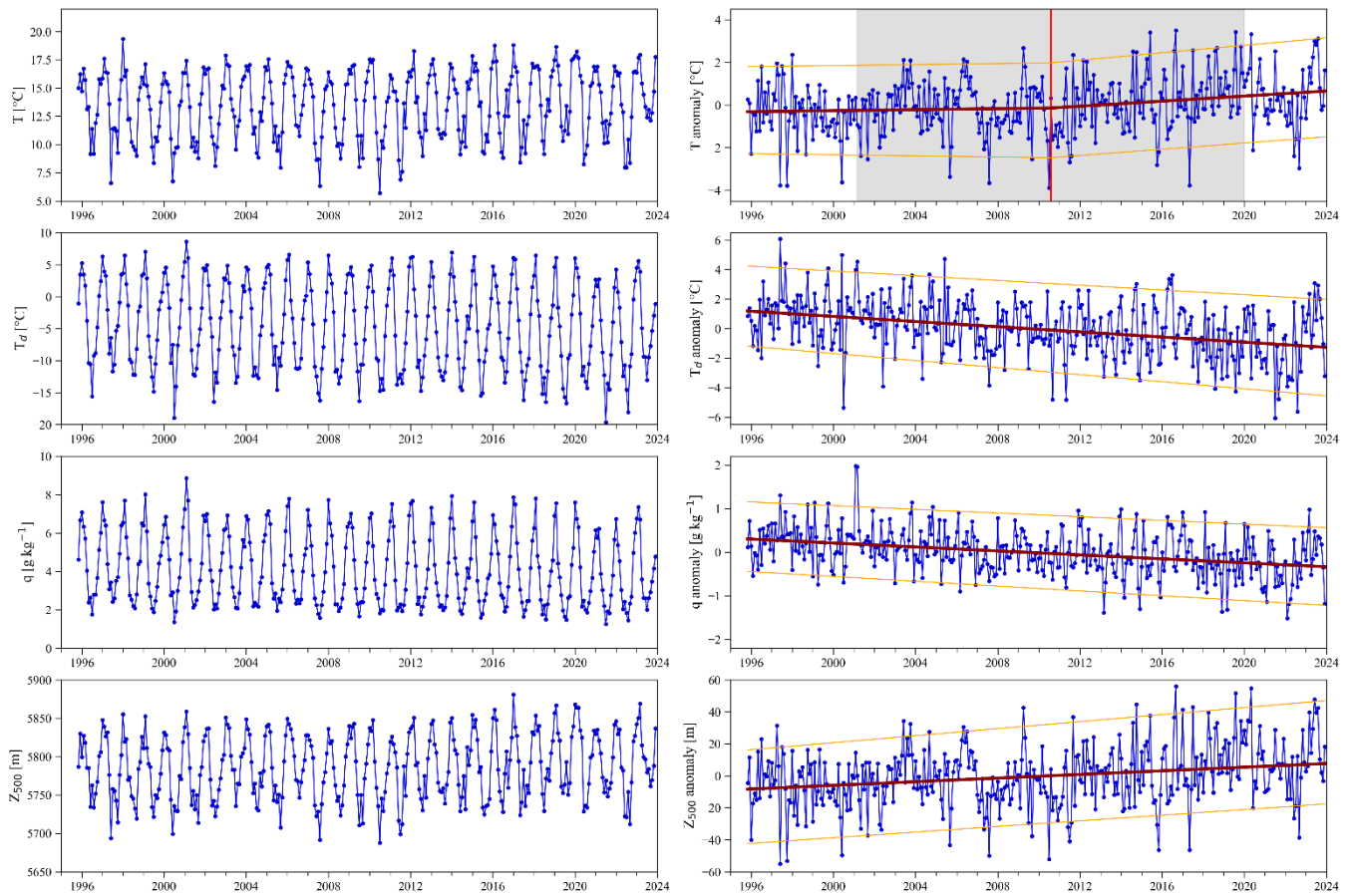
23 In Figure 2, CO shows two points of change around 2009 and 2014, which, we hypothesize may be linked to an
24 increased frequency and extent of fires in Central and Southern Chile (Carrasco-Escaff et al., 2024; González et al., 2018).
25 However, we cannot rule out that the use of a combination of model and instrumental data may yield spurious results. Our fire
26 hypothesis is based on the occurrence of large fires whose emissions of CO may reach Tololo, like in the summer of 2017
27 (Lapere et al., 2021).



1
2
3
4
5
6
7
8
9
10
11
12

Figure 2. The left panels show the monthly time series of ozone measured at Tololo, and monthly time series of reconstructed (See text for details) methane (CH₄) carbon monoxide (CO). The right panels show the corresponding seasonal anomalies, and the deseasonalized smooth trend for methane. The dark red line indicates the trend of 50th percentile and the orange lines indicate the trends of 5th and 95th percentiles. The vertical red line indicates change detected points and the gray shaded area shows its 95% confidence interval.

Methane shows three change points around 2000, 2006 and 2016 (Cf. Figure 2). In late 1999 a plateau in CH₄ mixing ratios started, following a period of steady increase and that remained for a few years until late 2006. This was observed around the world but the reasons that explain these changes are still subject to debate due to the complex interactions between emissions and chemistry that drive atmospheric methane (Saunois et al., 2020). We identify a trend change in 2016 which coincides with observed but still not fully explained changes in CH₄ growth rate (Nisbet et al., 2019).



1
2
3
4
5
6

Figure 3. The left panels show monthly time series of temperature (T), dew point temperature (Td), specific humidity (q) and geopotential height in 500 hPa (Z500) provided by ERA5 reanalysis and corrected by in situ observations, when available (See text for details). The right panels show the corresponding anomalies for temperature, dew point temperature, specific humidity and geopotential height at 500 hPa. The dark red line indicates the trend of 50th percentile and the orange lines indicate the trends of 5th and 95th percentiles.

7
8
9
10
11
12
13

A strong seasonality in all meteorological variables is apparent in Figure 3. The strong contrast between summer and winter values is characteristic of the subtropics (Garreaud et al., 2009). Except temperature that shows a change point around 2010 but with a broad uncertainty span, none of the variables shown in Figure 3 show clear changes in trends. Nevertheless, Central and Southern Chile experienced a continuous drought from 2010 to 2022 (Garreaud et al., 2020), which was interrupted by significant precipitation events over the latest winters. The changes in temperature and humidity observed at Tololo also reflect these conditions. This is in fact consistent with the warming and drying trends driven by climate change over Central and Southern Chile (Bozkurt et al., 2019).

14
15
16

As methane is the variable with the most noticeable upward trend, we assess the changes in hourly ozone distribution over time when methane changes. To this end, we consider four periods as inferred by the change points of methane. This is shown in Figure S 5. Until 2006, the mean and median of ozone only show a slight difference, while after 2006 these statistical

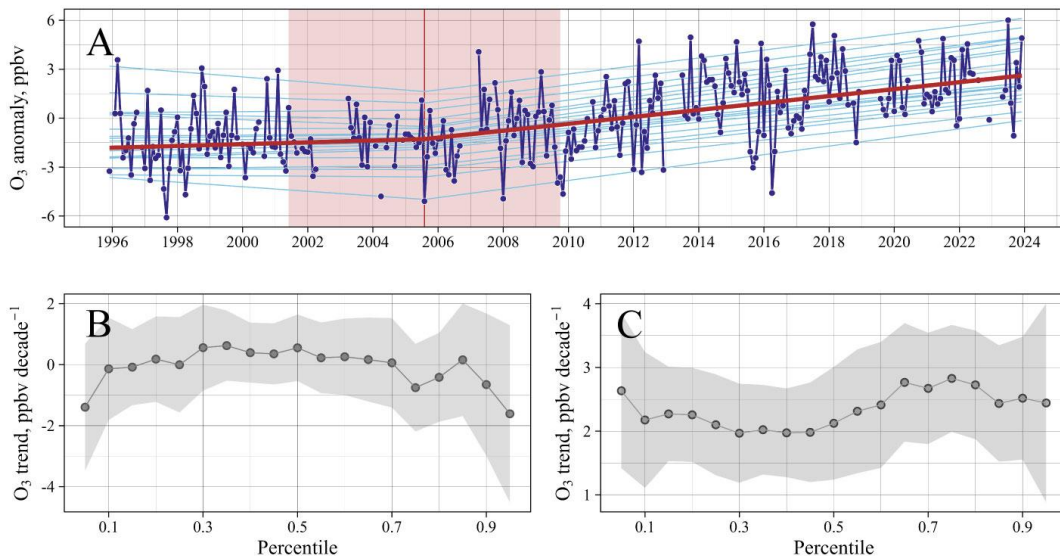
1 indicators clearly increase. Moreover, the growth in the indicators appears to accelerate further after 2016. This suggests that
 2 methane is a major driver of ozone changes at Tololo.

3 Next, we provide an update of the trend estimate presented by Seguel et al. (2024), including the determination of
 4 change points, all according to TOAR II recommendations (Chang et al., 2023). This is shown in Table 1 and Figure 4. Table
 5 1 shows that O₃ trends were negative or slightly positive before August 2005 for all percentiles, albeit with low reliability as
 6 defined by TOAR II. After the change point, a clear upward trend emerges for all percentiles (very high certainty). As
 7 previously indicated, trends at 5th and 95th percentiles are somewhat higher than the median trend, which may be indicative of
 8 the impact of extreme events, such as fires.

9 Table 1. Ozone trends and reliability (according to TOAR recommendation) are estimated for Tololo (5th, 50th
 10 (median) and 95th percentiles) over the period December 1995-December 2023. The table also shows year and month of the
 11 change point as well as the signal-to-noise ratio (SNR), the corresponding probability value (p Value), and the reliability of
 12 the estimate.

Percentile	Change Points	Trend ppbv / decade [± CI]	SNR	p Value	Reliability
5	Before August 2005	-1.4 [2.0]	-1.36	1.79E-01	Low certainty
50		0.4 [1.1]	0.85	3.97E-01	
95		-1.5 [2.9]	-1.06	2.94E-01	
5	After August 2005	2.7 [1.2]	4.54	3.11E-05	Very high certainty
50		2.1 [0.8]	4.85	1.07E-05	
95		2.5 [1.6]	3.11	2.93E-03	

13



1
 2 **Figure 4. Percentile trends derived by quantile regression applied to the deseasonalized monthly surface ozone at Tololo.**
 3 **In panel (A), the blue dots and light lines show the monthly anomalies of ozone at Tololo, the red line corresponds to the trend of**
 4 **the 50th percentile, and the light blue lines correspond to the trends of the remaining percentiles. The change point is represented**
 5 **by a vertical red line, and the shaded red area shows the corresponding uncertainty at the 95% confidence interval. Panels (B),**
 6 **and (C) show the percentile trends of the quantile regression from the 5th to 95th percentiles at 5 percentile intervals before and**
 7 **after the change point, respectively.**

8 **3.2 Influence of air of stratospheric and upper tropospheric origin intrusions**

9 We identified events of air of stratospheric and upper tropospheric origin (SUTO) as those characterized by high
 10 ozone and low humidity, possibly linked with stratospheric intrusions or downward transport of upper troposphere air as
 11 events of concurrent positive anomalies in ozone and negative anomalies in water vapor mixing ratio as described in Section
 12 2.6. Using said method, we found 336252 SUTO events stratospheric intrusion events over the period 1995-2023, of which
 13 roughly half 94 (17037%) last 24 hours or less, 122-103 (3640%) last between 24 and 48 hours, 33-35 (1014%) last between
 14 48 and 72 hours, and 11-20 (58%) last more than 72 hours (Cf. Figure 5). Median anomalies in ozone are around 5 ppbv and -
 15 2 g/kg in water vapor, which are significant magnitudes compared with typical ozone and water vapor values at Tololo.

16 While stratospheric intrusion-SUTO events can occur any month of the year, most of them take place during the cold
 17 season and early spring, between May and October. One can observe a distinct interannual variability in the number of events
 18 per year. Typically, there are fewer (more) intrusions-events in connection with the cold (warm) phase of ENSO, which is
 19 consistent with a stronger (weaker) South Pacific High that readily hinders (allows) the arrival of mid-latitude synoptic
 20 disturbances such as cutoff lows and deep troughs. There is no trend in the number of events per year nor in their duration.
 21 Furthermore, the number and duration of intrusion events do not appear to be related to the intensity of the ENSO anomaly
 22 (not shown).

At first sight, the fact that there are more intrusions-SUTO events in El Niño years might seem contradictory with the fact that the spring maximum in ozone at Tololo is typically larger during La Niña years rather than during El Niño years as firstly stated by Anet et al. (2017), and reproduced here (See Figure S 6). However, one must recall that several processes are at play stratospheric intrusions are not the only mechanism influencing ozone in Tololo. It is worth noticing that the model also captures the difference in ozone seasonality during El Niño and La Niña years, however the magnitude is overestimated (See Figure S 7).

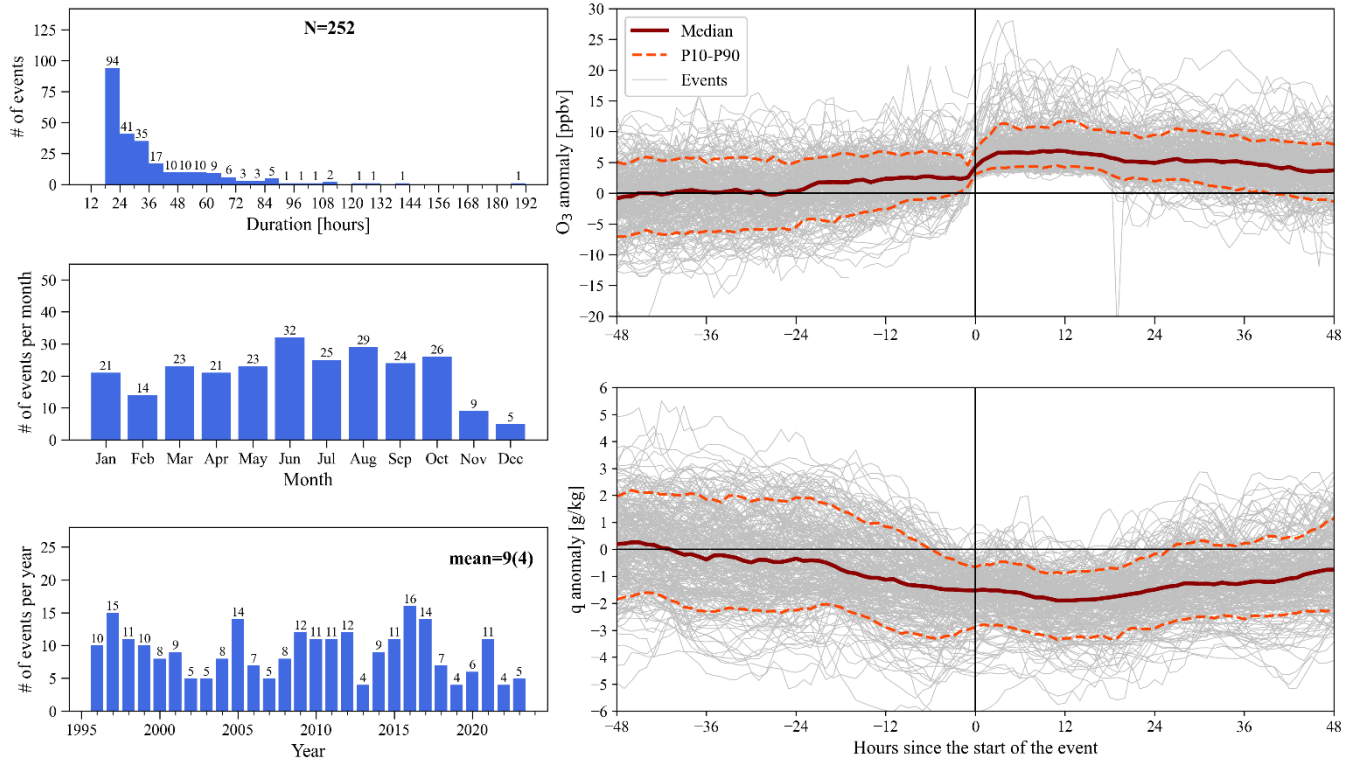
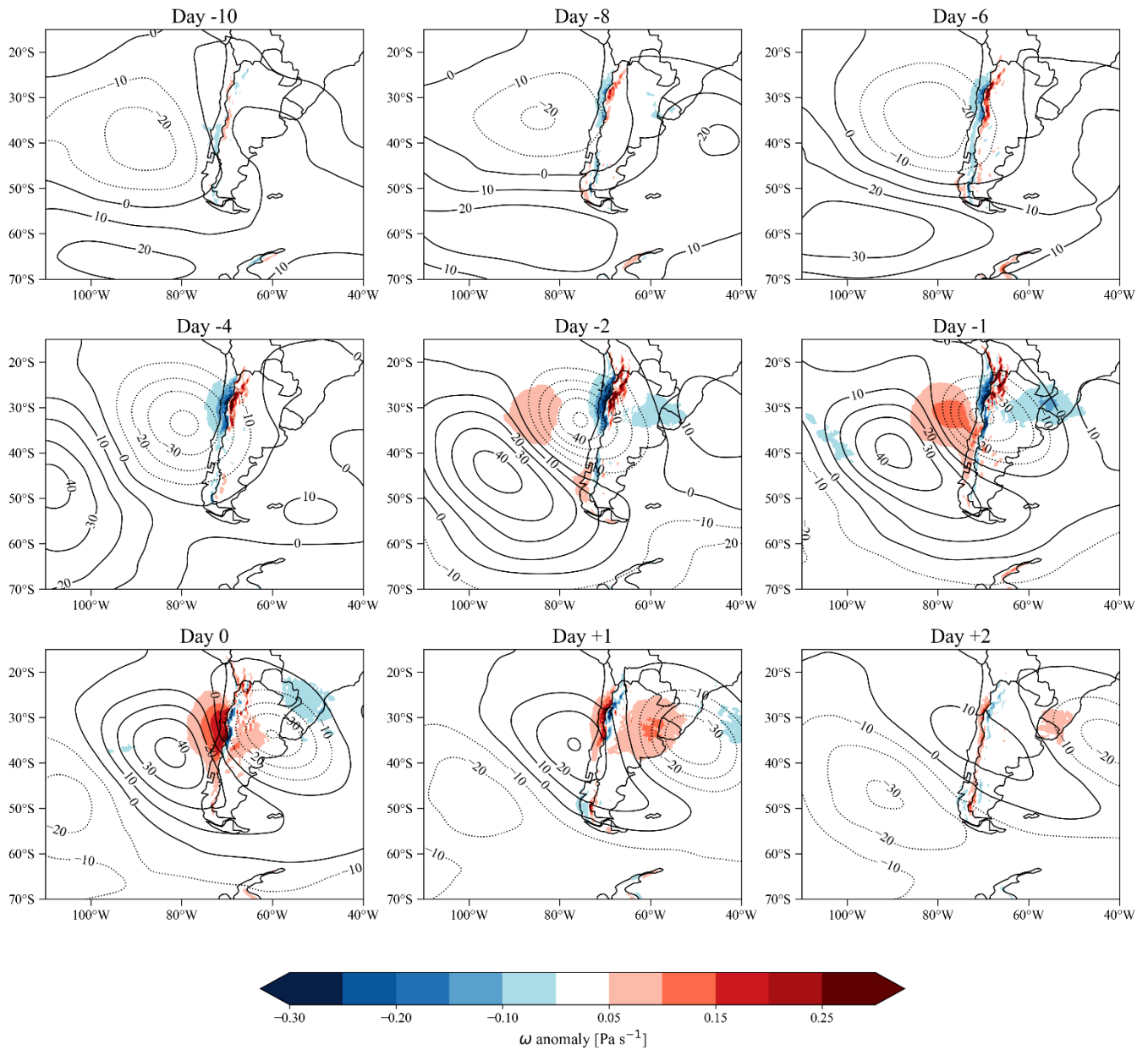


Figure 5. SUTO events Stratospheric intrusion events as detected at Tololo according to anomalies in ozone (positive) and water vapor (negative). The upper left panel shows the number of events according to duration in hours. The middle-left panel describes the seasonal distribution considering all events occurring in each month. The bottom left panel indicates the number of events per year between November 1995 and December 2023. To the right we show the behavior of each intrusion event (grey thin lines) as well as their statistics per percentile: 10 (dashed orange line), 50 (dark red line) and 90 (dashed orange line). The upper (lower) right panel shows the statistics for ozone (water vapor mixing ratio).

In addition to counting intrusion-SUTO events, we characterized their synoptic scale evolution. Figure 6 and 7 show composite anomalies in synoptic meteorological fields over a 12-day period that starts 10 days prior and ends 2 days after the stratospheric intrusion event. In the horizontal we show composite anomalies in geopotential height at 500 hPa, and vertical velocity (Figure 6). These fields show a slow passing deep trough of north-west to south-east orientation that reaches north of 30°S 10-days prior and shows a full mature stage by day -4. While the trough is approaching the Chilean coast, one observes

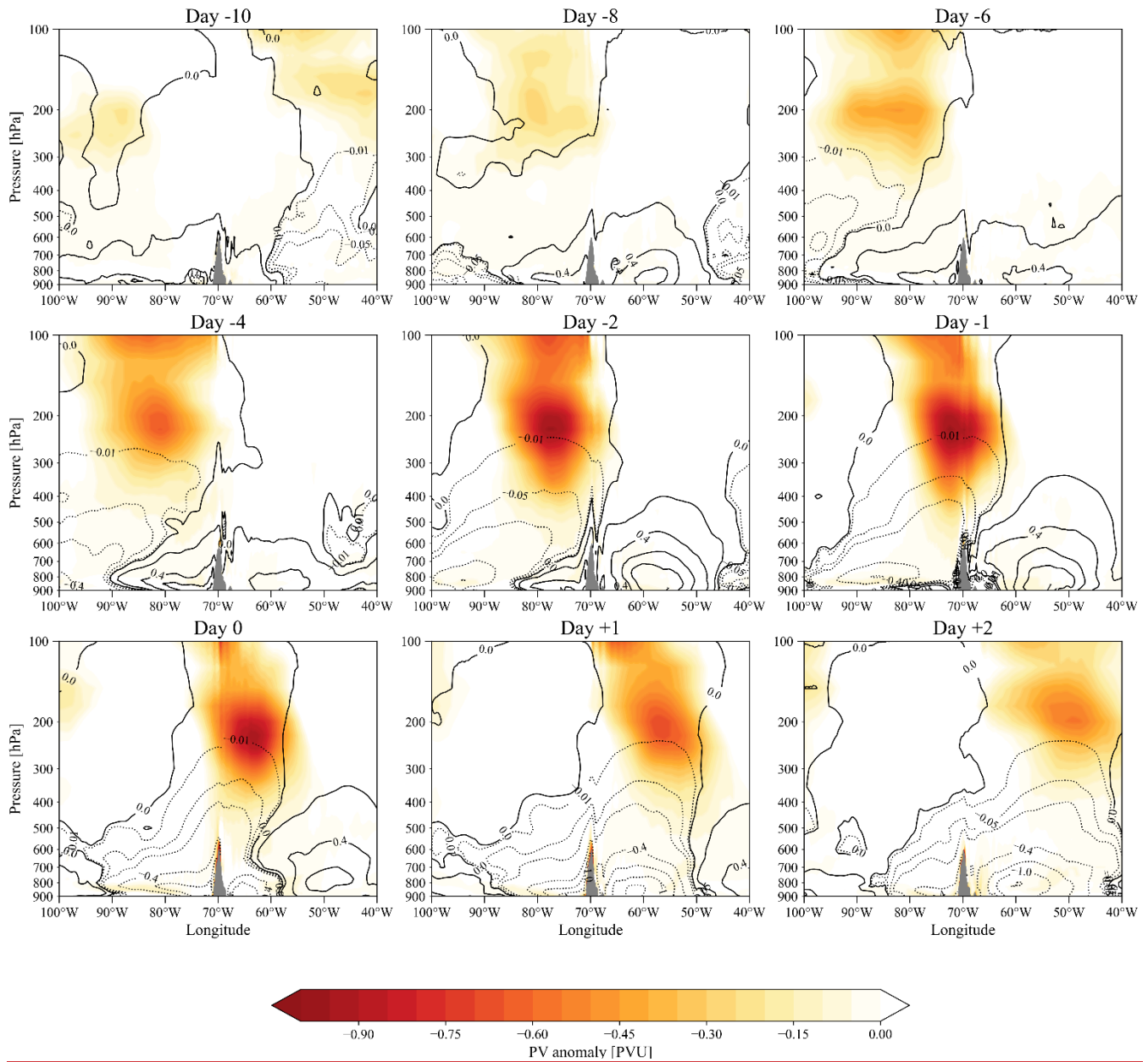
1 uplifting (subsidence) west (east) of the Andes, which is consistent with the behavior of deep troughs and cutoff lows
2 (Rondanelli, 2025). Thereafter, a subsidence zone is evident and advances eastward from day -2 to day 0, while a ridge
3 develops and the subtropical high-pressure system is re-established. Thus, there is subsidence upwind and passing over Tololo
4 with vertical velocity anomalies of more than 0.15 Pa/s, i.e., producing favorable conditions for stratospheric or upper
5 tropospheric ozone mixing down to Tololo. Furthermore, such configuration is consistent with the occurrence of stratospheric
6 intrusions upwind of Tololo. Nevertheless, the mere synoptic configuration does not assure the occurrence of STE.



1

2 **Figure 6. Composite maps of geopotential height and vertical velocity anomalies at 500 hPa during SUTO stratospheric**
 3 **intrusion**-events. Contours denote geopotential height anomalies in meters, where positive (negative) anomalies are solid (dotted)
 4 contours. Shaded areas denote vertical velocity anomalies in Pa/s.

5



1
 2
 3
 4 **Figure 7. Composite of longitude-pressure cross-section of potential vorticity and specific humidity anomalies between 900**
 5 **and 200 hPa during stratospheric intrusion-SUTO events. Contours denote specific humidity anomalies in g/kg, where positive**
 6 **(negative) anomalies are solid (dotted) contours. The shaded area denotes potential vorticity anomalies in potential vorticity units**
 7 **(PVU).**

1 It is well known that stratospheric air in the Southern Hemisphere is characterized by negative vorticity, and low
2 humidity. Therefore, in Figure 7, we show composite anomalies of potential vorticity and specific humidity of SUTO
3 stratospheric intrusion events. Consistently with the synoptic patterns discussed in Figure 6 but occurring ca. 48 hours prior,
4 the development of the deep trough is accompanied by the entrance of negative anomalies of potential vorticity and humidity
5 that propagate downwards, starting to reach Tololo already by day -2, i.e., prior to the maximum occurrence of positive ozone
6 and negative humidity anomalies. This is consistent with the duration of the events that typically last less than 3 days (>80%)
7 of the cases). Thereafter, the intruding air follows the westerlies with continued negative anomalies in potential vorticity and
8 humidity east of the Andes.

9 Hence, based on the observed data, synoptic conditions corresponding to the average of 252 cases show passing
10 troughs that reach the subtropics, which in turn are consistent with the potential occurrence of stratospheric intrusions. Said
11 conditions -events-lead to increases in ozone of around 5 ppbv on average at Tololo within a range between 3 and 12 ppbv,
12 accompanied by negative anomalies in humidity of around -2 g/kg, which in turn compare with typical ozone and water vapor
13 mixing ratios of 30 ppbv and 7 g/kg, corresponding to 17% and 28% respectively. Such events occur mainly in the cold season
14 and early spring and are favored by El Niño conditions. Said intrusions SUTOs typically occur in connection with deep troughs
15 and cutoff lows that connect the subtropics with higher latitudes. On average, one finds 12-9 events per year but within a broad
16 range between 4-5 and 23-13 events per year. The maximum ozone anomaly observed in our results corresponds to 15 ppbv,
17 this is low compared with values observed in the Northern Hemisphere. We attribute this to the generally stronger STE
18 observed in the Northern Hemisphere compared to the Southern Hemisphere (e.g., Holton, 1990).

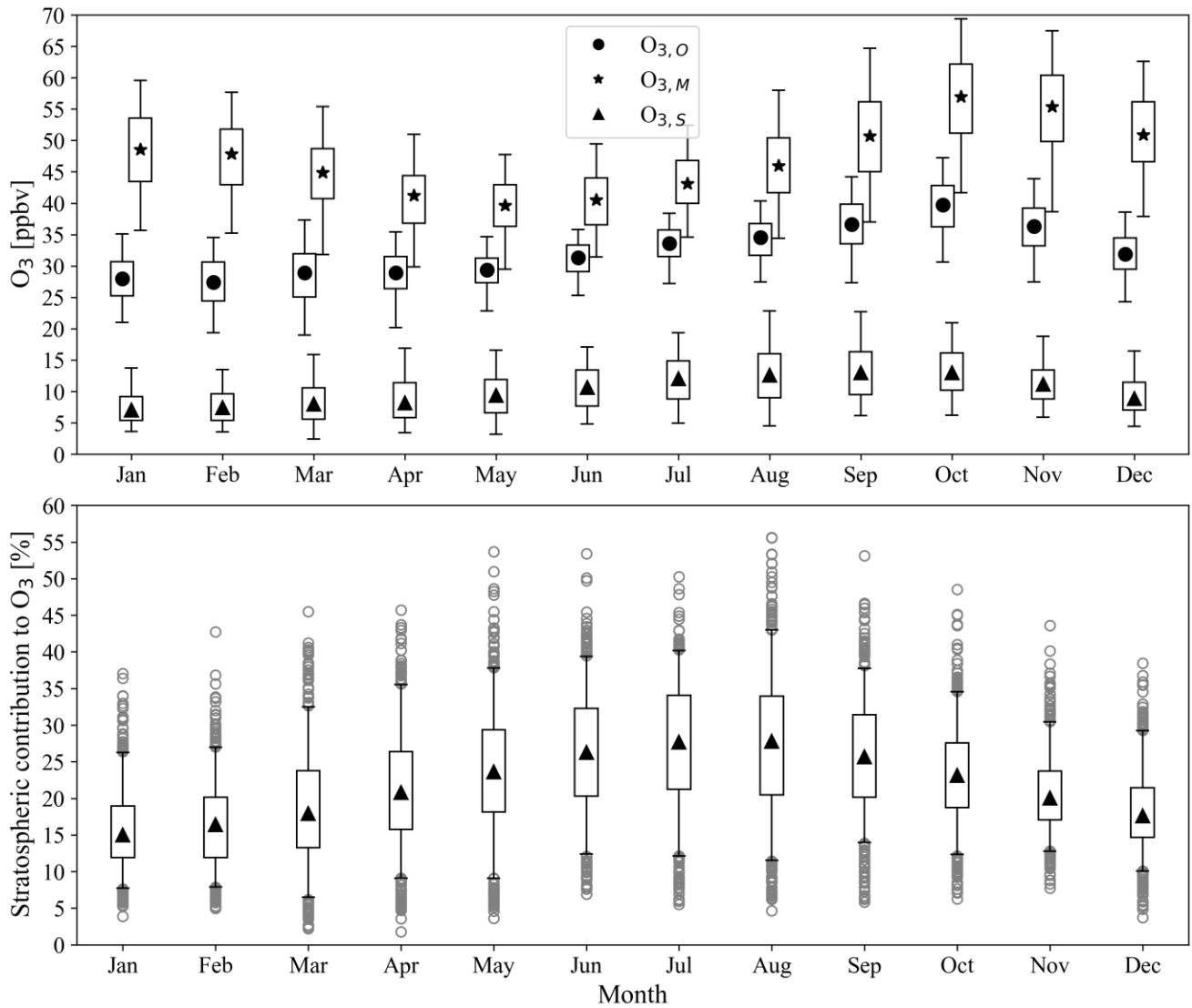
19 As indicated in the precedent paragraph, Figures 5 and 7 show a composite of 252 cases reflect that most of the cases
20 correspond to passing troughs. However, the average also includes other synoptic configurations. To better grasp this diversity
21 of cases, we performed a clustering analysis (k-means) to identify underlying structures, i.e., four groups of different synoptic
22 configurations, all leading to SUTO, and some clearly consistent with stratospheric intrusions occurring at different locations.
23 These clusters and the corresponding configurations are shown in Figures S 8 to S15. Three out of the four groups show
24 approaching or passing deep troughs or cutoff lows, and one denotes the presence of a zonal flow. Deep troughs show enhanced
25 subsidence behind the low-pressure system, some of which might be accompanied by a tropopause folding. In fact, part of the
26 back trajectories for the representative cases (maximum ozone anomalies) of the three groups showing trough configurations,
27 clearly indicate stratospheric intrusions, i.e., crossing of PV=-2 units (See Figures S 16 to S 20). Interestingly, the highest
28 ozone anomaly (≈ 15 ppbv) event takes place in connection with a defined jet-stream, which in addition to transporting upper
29 troposphere air eastwards, it trickles down stratospheric air possibly by marked turbulence associated with the jet-stream.

30 The TM4-ECPL model also provides an estimate of the stratospheric influence on Tololo ozone (Figure 8). In these
31 simulations, the ozone of stratospheric origin reaches Tololo all year around but in winter and early spring (June through
32 September) this contribution surpasses 10 ppbv (on average), and in summer (December through February) it is roughly half
33 of that. This corresponds to a percentage contribution of roughly 15% in summer to 25% in winter. It is worth noting that the
34 seasonality of the stratospheric contribution found in the simulations is largely consistent with the seasonality found for SUTO

1 ~~events through our methodology~~ and shown in Figure 5, i.e., the model captures the overall seasonal variability of ozone with
2 higher values in winter and early spring than in summer and early fall. However, an overestimate of ozone at Tololo by nearly
3 a factor of two is evident. Moreover, there are many days with stratospheric contributions that reach or surpass 50% of the
4 estimated ozone in winter (Cf. Figure 8). We suspect that part of the mismatch between model and observations is due to too
5 strong a stratospheric contribution. In its current version, the upper boundary condition for O₃ is estimated by nudging O₃
6 concentrations above 50 hPa altitude to satellite observations with no explicit stratospheric chemistry. This was already
7 reported when evaluating TM4-ECPL against ozone soundings at Rapa Nui, where an overestimate of ozone in the upper
8 troposphere was found (Daskalakis et al., 2022).

9 In Figure 9 we show the number of days of stratospheric intrusions and their contribution to ozone as calculated by
10 TM4-ECPL for the period 1995-2015, categorized by season. Also, we indicate the number of events that coincide with those
11 detected by our empirical methodology. The total number of days estimated by TM4-ECPL is typically an order of magnitude
12 higher than the number of days ~~when stratospheric intrusions were~~ SUTO events detected, particularly in summer, which
13 again suggests too strong a stratospheric contribution all year. Also, TM4-ECPL estimates many days with stratospheric
14 contributions of less than 5 ppbv, whereas the concurrently observed ~~intrusions~~ SUTO events do not. The largest stratospheric
15 contributions estimated by TM4-ECPL reach 40 ppbv or 35 ppbv when considering only days when we observed
16 ~~intrusions~~ SUTO events, which is in any way much larger than the ozone anomalies based on the empirical method that reaches
17 up to ~~25-15~~ ppbv. Lastly, the median stratospheric contributions calculated with TM4-ECPL are around 15 ppbv per day but
18 that of the empirical method is only 5 ppbv.

19



1

2

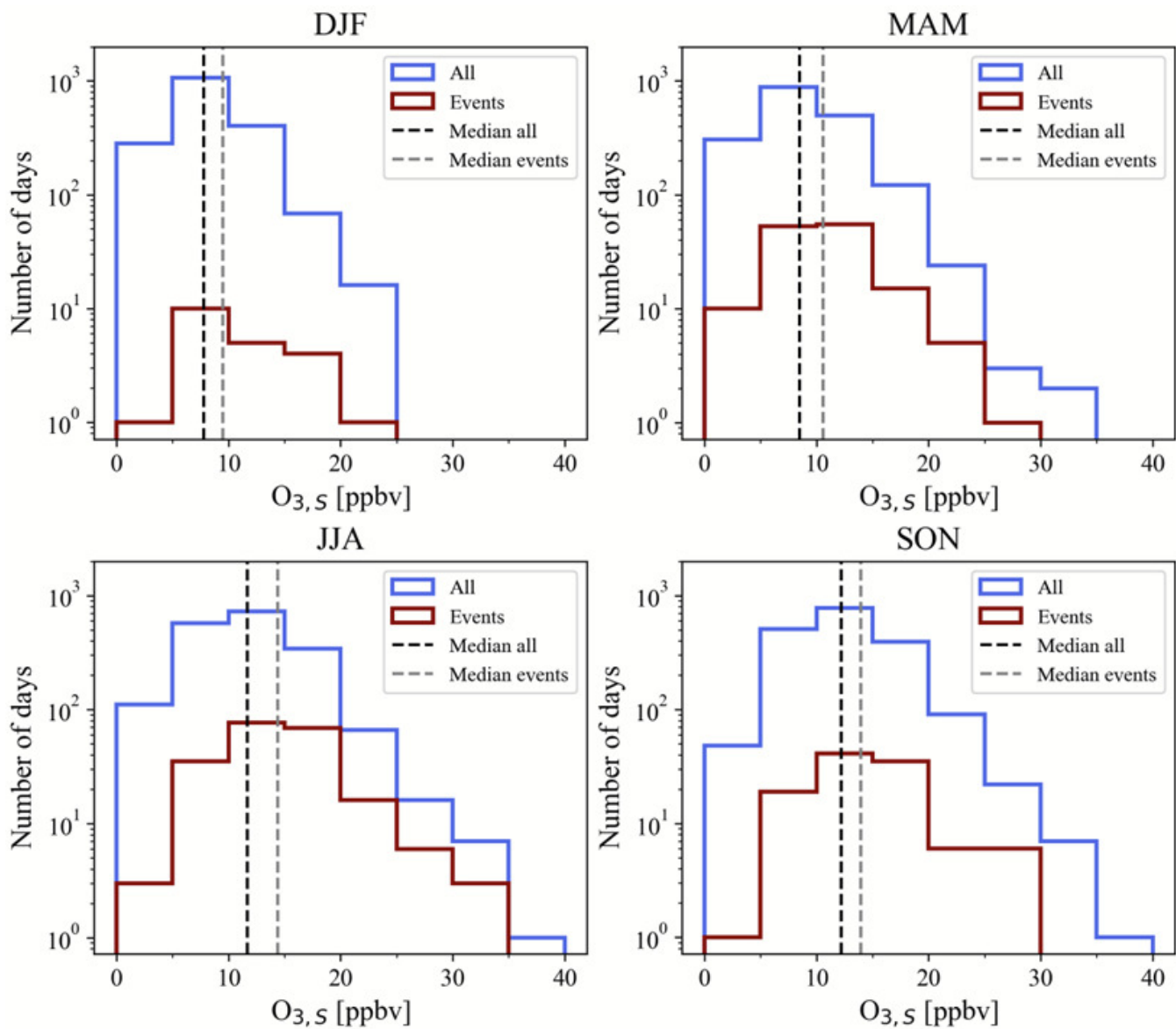
3

4

5

6

Figure 8. Contribution of stratospheric ozone at Tololo. In the upper panel we show the average seasonal variability as boxplots of observed ozone ($O_{3,o}$), simulated ozone ($O_{3,M}$) and simulated stratospheric ozone contribution ($O_{3,s}$). The lower panel shows the corresponding percentage of stratospheric contributions to ozone. The whiskers indicate 5th and 95th percentiles of data distributions. We show outliers as grey circles only in the lower panel. Boxplots were constructed for the period between November 1995 and January 2015. Simulations correspond to TM4-ECPL outputs.



1

2

3

4

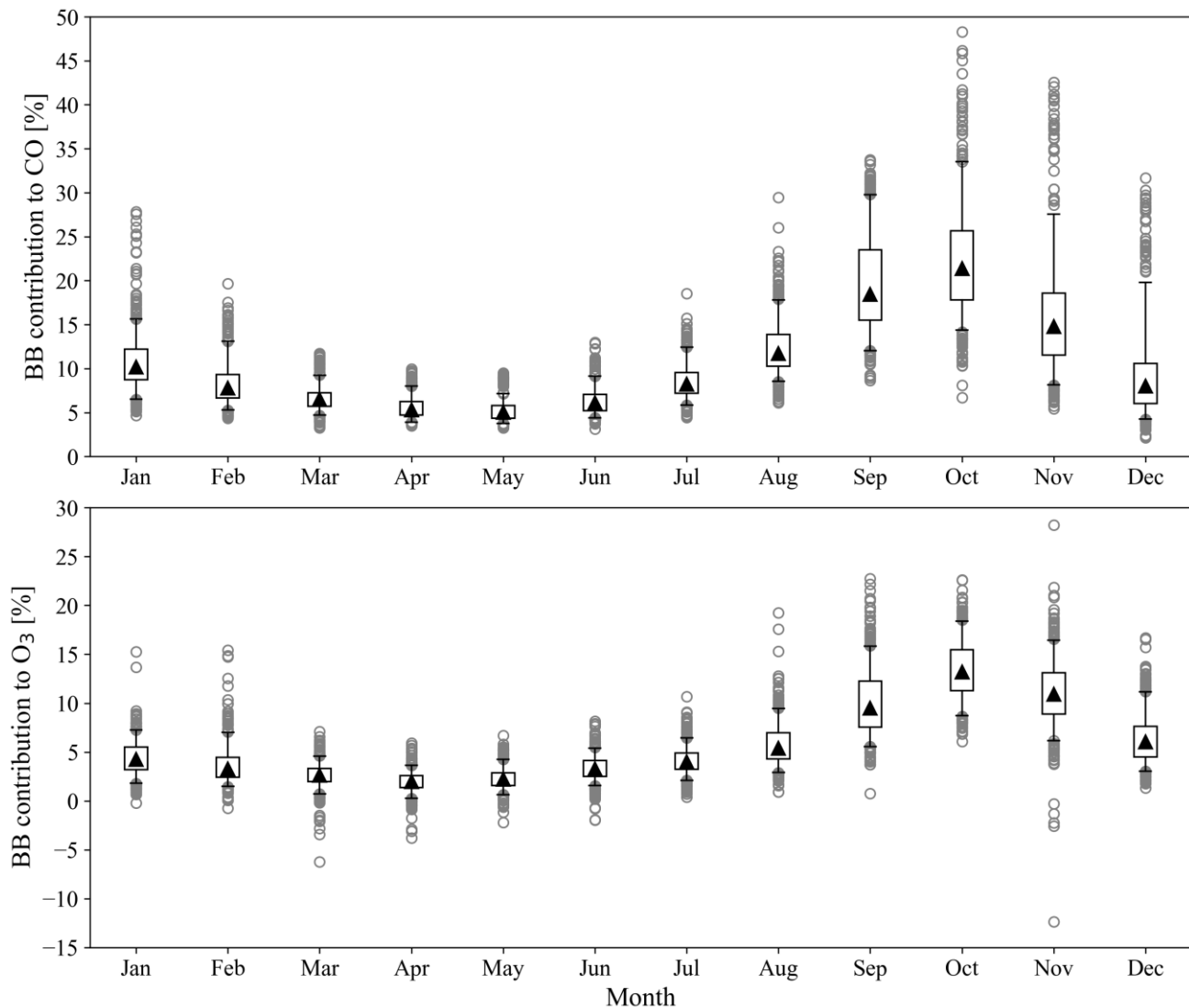
5

6

Figure 9. Seasonal daily stratospheric ozone contributions ($O_{3,s}$) at Tololo according to the TM4-ECPL model. In blue we show the distribution of all events calculated by the model. In red, we show the -eventsoccasions that coincide with intrusion-SUTO events as determined by the empirical methodology. Each panel shows the corresponding histogram for summer (DJF), fall (MAM), winter (JJA) and spring (SON). Vertical dashed lines indicate the median of the distributions.

3.3 Influence of biomass burning

As shown in Figure S 4, CO at Tololo was overestimated by the model simulation by on average about 7 ppbv over the period when we count with both observations and simulations (2013-2015). We corrected this by applying a bias correction method (Cannon et al., 2015; Staehle et al., 2024) to reconstruct the whole model series (1995-2015). The contribution of biomass burning to CO and ozone was calculated as the difference between the runs with and without biomass burning as shown in Figure 10. The role played by biomass burning in terms of ozone production and transport over the east Pacific – particularly during spring– has been shown in earlier work (e.g., Daskalakis et al., 2022). This influence is also clear in Tololo where an increase in CO during spring is both simulated and observed (See Figure S 2). While observations of CO do not allow attributing the biomass signal, simulations do. According to the TM4-ECPL model outputs, i.e., with all sources and without biomass burning, the seasonally averaged contribution to ambient CO at Tololo reaches up to nearly 23% in October. The minimum contribution occurs in April when the average is about 5%. Notice that in summer (DJF), averaged values of biomass burning contributions are lower than in spring, but one observes a secondary maximum in connection with regionally occurring fires that have become more common over central and southern Chile (e.g., Lapere et al., 2021). Regarding ozone, the biomass contribution peaks also in October, but it only reaches a median value of about 15% of total ozone (~35 ppbv).



1

2 **Figure 10. Biomass burning (BB) contribution to CO (upper panel) and ozone (lower panel) as calculated by the TM4-**
 3 **ECPL model. Monthly averages are calculated over daily values. Whiskers indicate the 5th and 95th percentiles of the data**
 4 **distributions. Outliers are shown as grey circles.**

5

3.4 GAM model

6

After trying several combinations of potential explanatory variables, we chose 14 as indicated in Table 2. This set of
 7 variables were chosen based on their physical meaning and relevance for explaining ozone and trying to identify largely
 8 independent variables. Thus, our GAM has the general expression (Eq. 2):

9

$$O_3 = \epsilon + f_1(T) + f_2(q) + f_3(v) + f_4(Wdir) + f_5(BLH) + f_6(STE\ duration) + f_7(ENSO) + f_8(QBO) +$$

10

$$f_9(MJO) + f_{10}(\omega) + f_{11}(CH_4) + f_{12}(CO) + f_{13}(DofW) + f_{14}(DofY) \text{ (Eq. 2)}$$

1 where ε represents an error term, and f_i , $i=1,14$ are spline functions, in this case with 9 nodes that represent the dependences –
2 potentially nonlinear– on different variables detailed in Table 2.

3 The model (GAM) aims at capturing daily average values of ozone. As seen in Figure 11, the model represents most
4 features of the time series, including day-to-day, seasonal and interannual changes. It captures 76% of the data variability but
5 it tends to underestimate extreme values. Still, on average, the error is less than 3.6 ppbv. Also, the model captures the trend
6 of the observed data, i.e., 1.0 ppbv/decade, using the Ensemble Empirical Mode Decomposition (EEMD) as described in Anet
7 et al. (2017). This trend is 30% larger than the one calculated by Anet et al. (2017), which is in line with increasing ozone
8 mixing ratios at Tololo. When we run GAM without considering the influence of methane, GAM estimates a trend for the
9 1996-2023 period of only 0.4 ppbv/decade, highlighting the significant role of methane in explaining the observed upward
10 trend in ozone at Tololo. Without methane both variance (74%) and error (3.7) show a slightly worse performance.

11 To assess the relative importance of the different variables we used two techniques. First, we calculated the partial
12 dependences of the GAM reconstructed ozone with respect to each variable. This is shown in Figure 12, and discussed here:

- 13 • The day of the year (seasonality) contributes the most to ozone with up to 8 ppbv in spring, and secondarily with ca. 3
14 ppbv in winter. Seasonality also contributes slightly (< 2 ppbv) but negatively to ozone at Tololo in fall. In summer, a
15 small increase in ozone appears. This seasonal variability is fully consistent with the processes we have previously
16 described: [STE-SUTO events](#) in winter and spring, biomass burning in spring, episodic fires over central and southern
17 Chile in summer, etc.
- 18 • The second largest contributing variable is absolute humidity. This relationship is inversely proportional between O_3 and
19 humidity, reflecting the fact that water vapor acts as a sink for ozone, particularly in the remote atmosphere. While dry air
20 is associated with higher ozone levels, wet air of marine origin is associated with lower ozone levels. The former is
21 consistent with the influence of free tropospheric air, potentially of stratospheric origin, which is typically linked to dry
22 or very dry air. The latter occurs in summer when the marine boundary layer grows, entraining wet and low ozone air, or
23 when deep troughs and sometimes cutoff lows reach the subtropics vigorously mixing up wet air.
- 24 • Regarding the influence of temperature, we find that low values ($< 5^\circ C$) result in a negative contribution possibly linked
25 to very stable atmospheric conditions including subzero temperatures and very stable conditions leading to dry deposition.
26 Higher temperatures ($> 5^\circ C$) show a positive relationship, largely linear with a contribution of up to 4 or 5 ppbv in ozone.
27 This type of relationship has been found in many places around the world in polluted areas and they are attributed to the
28 increase of reaction rates with temperature, as well as to more intense solar radiation and increases in biogenic VOC
29 emissions (Porter and Heald, 2019; Szopa, 2021). At Tololo, such phenomena cannot be ruled out however the magnitude
30 of the relationship is much smaller than the one found in the polluted conditions of Santiago (not shown). Moreover, the
31 graph showing the day of the week shows no significant changes in ozone during the week, in other words there is no
32 weekend-effect as typically found in urban areas and suggestive of local ozone precursors (Seguel et al., 2012).
- 33 • Boundary layer height has a clear positive influence on ozone up to 400 m, thereafter its impact declines and becomes
34 negative for heights above 800 m. A growing boundary layer may result in the downward mixing of O_3 rich air from the

1 free troposphere, however too deep a boundary layer is suggestive strong vertical mixing and intrusion of marine air that
2 is typically O₃ poor, a phenomenon already described in connection with the description of the effects of humidity.

- 3 • A distinct although somewhat noisy positive contribution to O₃ is attributed to the duration of stratospheric intrusions as
4 defined in this work, which is to be expected under those circumstances. A similar result was found when using potential
5 vorticity: the more negative (more stratospheric) it is, the larger the contribution to O₃. To avoid including two equivalent
6 indicators, we decided to include the simpler duration indicator.
- 7 • Our ENSO indicator (MEI) has overall a positive impact on ozone, and more markedly so during La Niña years. In
8 connection with La Niña years, one expects stronger subsidence able to transport upper ozone rich air towards Tololo.
9 During El Niño years, the subtropical high is weakened, and more synoptic systems may arrive at Tololo. Thus, despite
10 the noisiness of the relationship between ozone and MEI, it appears physically sound.
- 11 • Variability sources like QBO and MJO show a minor contribution (< 2ppbv) to O₃. The phase of MJO shows a rather
12 discrete maximum at phase 5 which is largely consistent with the observations by Barrett et al. (2012), who found a
13 maximum in ozone for phase 6 of MJO in Santiago, i.e., still in the subtropics of Chile. This coincides with active
14 convection over the western Pacific and a strengthened Pacific high over the eastern Pacific. The influence of QBO appears
15 to be small with relative maxima with either Westerly or Easterly winds in the stratosphere. This might be because Tololo
16 is only at 2151 m a.s.l., which makes it difficult for a stratospheric signal to be clearly distinguished. Still, one must keep
17 in mind that when contributions are small there is the risk of over-interpreting potential statistical artifacts.
- 18 • Wind direction shows a positive contribution (up to 1 ppbv) that is maximized on westerly winds (250 degrees) that bring
19 air from the Pacific that in spring transports the biomass signature that is rich in O₃ and O₃ precursors. Also, northerly
20 winds show a maximum that may occur in connection with midlatitude disturbances that are often associated with
21 subsidence behind the low-pressure system and sometimes tropopause breaks. However, these contributions are small,
22 and they might be statistical artifacts. The dependence on wind speed is rather flat over the range between 0 and 12.5 m/s,
23 but slightly positive, which again might be linked to the passage of synoptic disturbances and their associated vertical
24 mixing.
- 25 • Positive omega velocity (subsidence) shows a relatively small (< 2 ppbv) influence on O₃, which is expected as the free
26 troposphere is generally richer in ozone than the lower troposphere. However, negative omega velocities also show a
27 minor positive contribution to O₃. This may be linked to the subsiding back side of synoptic perturbations.
- 28 • According to our GAM, methane contributes positively to ozone with CH₄ mixing ratios above ~1725 ppbv, and slightly
29 negative below that value, which roughly coincides with the first methane change point shown in Figure 2. There is an
30 inflexion point in the contribution when methane surpasses 1780 ppbv and approaching 1800 ppbv the contribution
31 increases to nearly 3ppbv with current methane levels. Again, this coincides with the change points of the methane time
32 series (Cf. Figure 2). This is consistent with what we have discussed regarding the role of methane in explaining the trend
33 observed in ozone at Tololo.

- 1 • CO shows a positive contribution above 75 ppbv, which coincides with the value observed in spring and linked to biomass
 2 burning transported over the Pacific. Above that level, the contribution of CO increases further.

3 Notice that all 50 runs of GAM showed similar functional dependences of the variables (See Figure 11) except for
 4 different error distributions among different variables. Thus, while the quantitative functional dependences may vary among
 5 runs, there is an overall physical consistency in those.

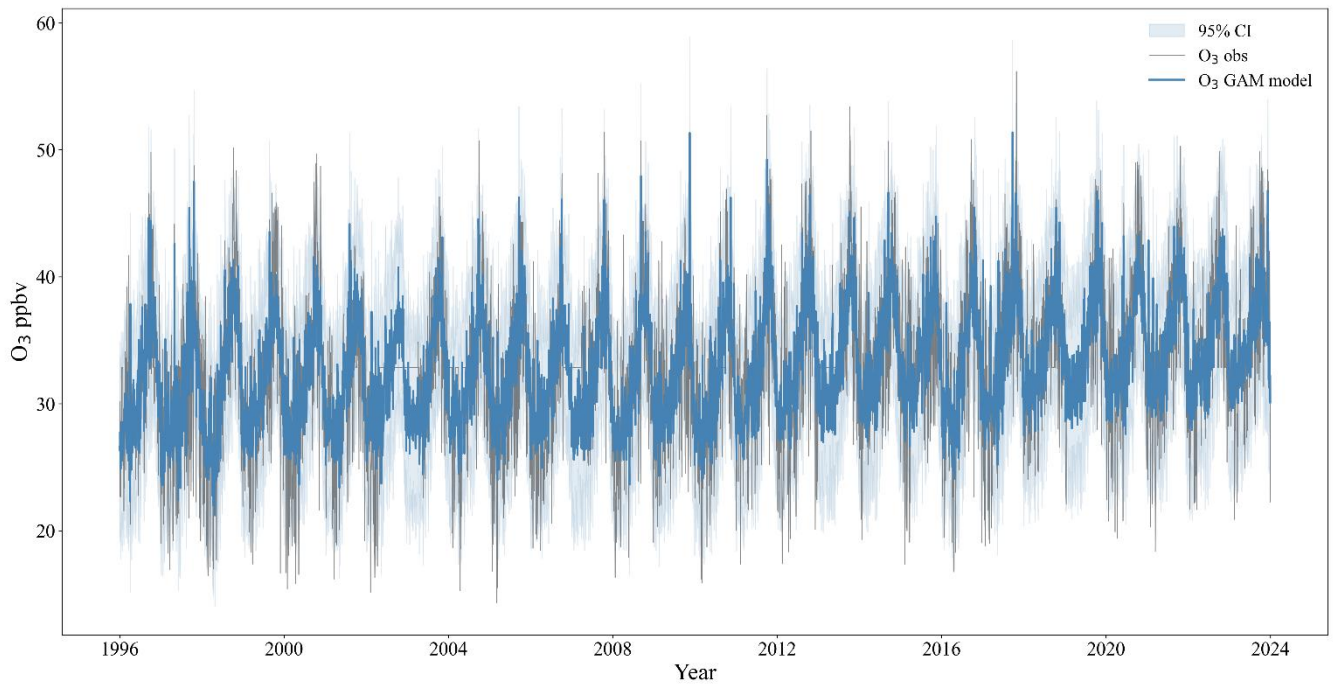
6

7 **Table 2. Chosen variables for GAM to explain ozone at Cerro Tololo. For sources of information and data please see the**
 8 **main text.**

Variable	Symbol	Units
<i>Local Meteorology (at 775 hPa)</i>		
Temperature	T	Degrees Celsius (°C)
Specific Humidity	Q	g/kg
Wind speed	v or Wind speed	m/s
Wind direction	Wdir or Wind direction	Degrees
Boundary layer height	BLH	m
Vertical velocity	Ω	Pa/s
<i>Synoptic Meteorology</i>		
Duration of STE	STE Duration	h
<i>Large-scale variability</i>		
El Niño/La Niña Southern Oscillation	MEI	PVU
Quasi Biennial Oscillation at 50 hPa	QBO	Nondimensional
Madden-Julian Oscillation Phase	MJO	Nondimensional
<i>Atmospheric Composition in situ</i>		
Observed methane combining Rapa Nui and Tololo series	CH ₄	ppbv
Carbon monoxide combining (bias correction) TM4-ECPL and observations	CO	ppbv
<i>Temporal variables</i>		
Day of the week	D-W	Nondimensional
Day of the year	D-Y	Nondimensional

9

10



1

2

3

4

Figure 11. Reconstruction of the ozone time series through GAM as described in the text. The ~~red-grey~~ values are daily averaged observations, and the ~~black-blue~~ ones are those of the GAM model. The ~~grey-blueish~~ line shows the 5th and 95th confidence intervals calculated by GAM.

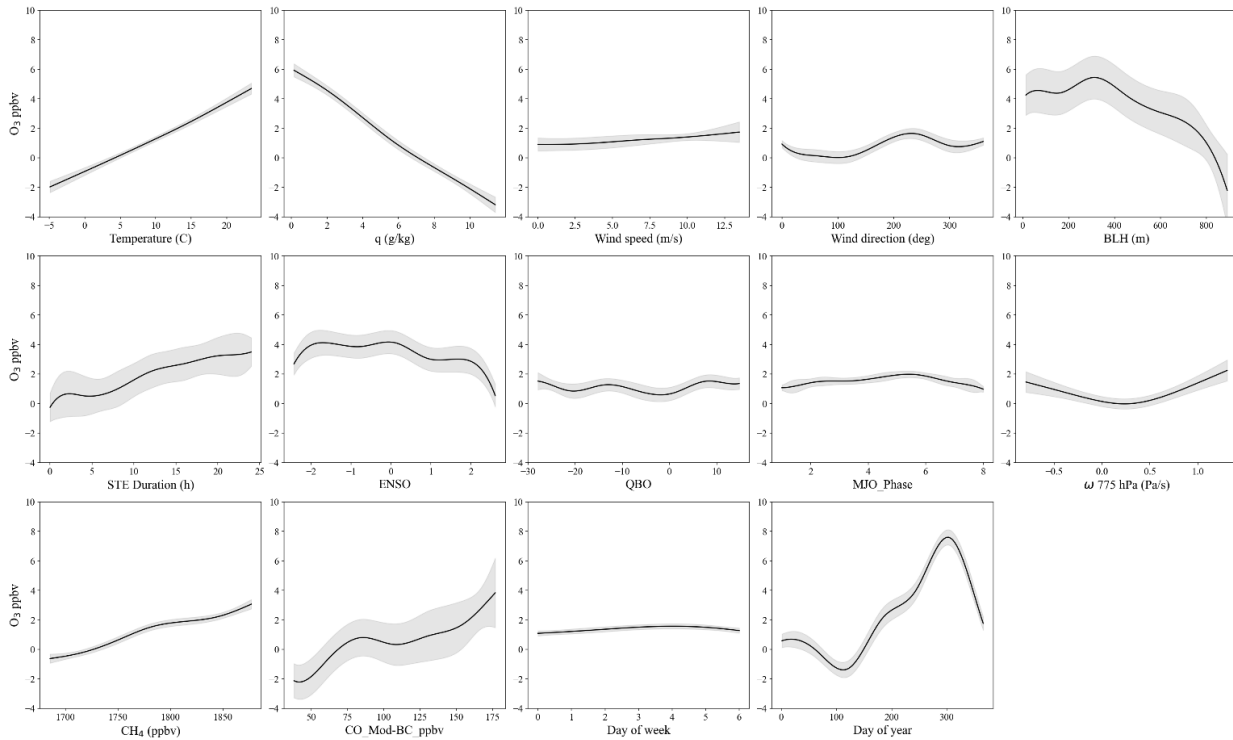


Figure 12. Partial dependences of the GAM reconstructed ozone on each variable.

The previous paragraphs describe the partial dependences found in GAM. Now we present the results of the SHAP method (See Figure S 207). Again, SHAP ranks seasonality, humidity, temperature, methane, carbon monoxide, and boundary layer height as the most important variables, following the physical reasoning described earlier. The same applies for the duration index. However, according to SHAP, El Niño years have mostly a negative influence on ozone, while La Niña years have a slight positive impact, which differs somewhat from the much smoother ENSO functional dependence shown in Figure 12. All other remaining variables are of less importance in SHAP. All in all, despite minor differences, the partial dependences of the GAM and the SHAP approach result in similar results in terms of the relative importance and role of the independent variables affecting ozone. This is encouraging as these methods have different mathematical grounds.

4. Summary and conclusions

In this work, we have studied ozone trends and variability at Tololo in the subtropics (mainly in the free troposphere) of the Southern Hemisphere. We used the TOAR methodological recommendations to detect change points and estimated linear trends per percentile between change points for ozone as well as for methane, temperature, specific humidity, dewpoint temperature, and geopotential height at 500 hPa which are potential explanatory variables for O₃. Ozone (median) shows a growing positive trend—~~median trend~~ both before and after 2006, the rate of growth being larger after 2006 (2.1±0.8

1 ppbv/decade, very high certainty) than before 2006 (0.4 ± 1.1 ppbv/decade, low certainty). The 5th and 95th percentiles indicate
2 decreasing trends before 2006 and growing trends thereafter suggesting a more significant influence of extreme events in the
3 later period.

4 Of all potential explanatory variables for ozone included in our GAM, methane accounts for the growing trend in
5 ozone. ~~This is also suggested by the~~ This is consistent with the concurrent changes in ozone and methane over the period 1996-
6 2023 (Figure S 5). However, this is difficult to reconcile with the long turn over time of ozone. Still, the ratio between ozone
7 burden and methane burden per year is within the range of values calculated by other authors using global models. While this
8 has been indicated in earlier work, our GAM approach provides a quantitative assessment of the association.

9 Knowing that ~~stratospheric intrusions~~ air of stratospheric and upper tropospheric air (SUTO) ~~are~~ is characterized by
10 relatively high O₃ and low water vapor mixing ratios, we used the hourly anomaly time series of O₃ and specific humidity at
11 Tololo to identify ~~said intrusions~~ SUTOs. We found ~~336-252 stratospheric intrusion SUTO~~ events over the period 1995-2023,
12 of which ~~94 roughly half (37%±70)~~ last 24 hours or less, ~~103±22 (40±6%)~~ last between 24 and 48 hours, ~~35±3 (140%)~~ last
13 between 48 and 72 hours, and ~~4±20 (58%)~~ last more than 72 hours (Cf. Figure 5). The composite patterns of these events
14 coincide with the approach of cutoff lows and deep troughs, reaching the subtropics at different locations upwind or over
15 Tololo. Hence, based on the observed data, ~~stratospheric intrusions~~ SUTO events, some of them clearly connected to STE, lead
16 to increases in ozone of around 5 ppbv (3 to ~~10±2~~ ppbv) on average at Tololo, accompanied by negative anomalies in humidity
17 of around -2 g/kg, which in turn compare with typical ozone and water vapor mixing ratios of 30 ppbv and 7 g/kg, i.e., 17%
18 and 28% respectively. In addition to a composite analysis, we also performed a clustering analysis that shows that three out of
19 the four groups show approaching or passing of deep troughs or cutoff lows, and one denotes the presence of a zonal flow.
20 Deep troughs show enhanced subsidence behind the low-pressure system, some of which might be accompanied by a
21 tropopause folding. In fact, part of the back trajectories for the representative cases (highest ozone anomalies) of the three
22 groups showing trough configurations, clearly indicate stratospheric intrusions, i.e. trajectories that cross the PV=-2 PVU.
23 While ~~stratospheric intrusion~~ SUTO events can occur any month of the year, most of them take place during the cold season
24 and early spring, between May and October. Typically, there are more ~~intrusions~~ SUTO events in connection with the warm
25 phase of ENSO, which is consistent with a weaker South Pacific High, allowing the arrival of mid-latitude synoptic
26 disturbances such as cutoff lows and deep troughs. There is no trend in the number of events per year nor in their duration.
27 The influence of stratospheric air was also assessed using a state-of-the-science atmospheric chemistry model (TM4-ECPL).
28 The model captures the seasonal variability in the stratospheric ozone contribution, but it calculates too strong an impact,
29 possibly due to the way it handles the upper boundary condition as identified in an earlier study.

30 According to the bias corrected TM4-ECPL model outputs, i.e., with all sources and without biomass burning, the
31 seasonally averaged contribution to ambient CO at Tololo reaches up to 23% in October. The minimum contribution occurs in
32 April when the average is about 5%. In summer, averaged values of biomass burning contributions are lower than in spring,
33 but one observes a relative maximum in connection with regionally occurring fires that have become more common over
34 central and southern Chile. The contribution of biomass burning to ozone peaks also in October, but it only reaches a median

1 value of about 15% of total ozone or about 5 ppbv. Hence, the contributions of biomass burning and SUTOs, including
2 stratosphere-to-troposphere transport of O_3 at Tololo, particularly during the late winter and spring ozone maximum are of
3 similar magnitude and in the order of 5 ppbv per event, with a broad range of variability.

4 To follow changes in atmospheric composition and ozone forcing in the free troposphere of the otherwise sparsely
5 observed Southern Hemisphere, Tololo has privileged location. It is typically immersed in the free troposphere and affected
6 by the subsidence regime of the South Pacific high that brings clear sky conditions, and in winter, the subtropical jet stream is
7 located on average at 30°S. In a rapidly changing climate, the expected intensification and expansion of the Hadley, and
8 possibly Walker, circulation can be followed from Tololo not only in terms of meteorological variables but through the
9 radiatively relevant ozone and methane. Thus, we argue that Tololo is a key background station to maintain and expand in the
10 context of a rapidly changing climate.

11
12 Author contributions. LG, ChO, CM: conceptualization; ND, MK atmospheric chemistry simulations; ChO, RR: composite
13 analysis; ChO, LC: Trend analysis; CM, LG: GAM methodology; CHO, KB, LG bias correction; ChO data curation; LG:
14 writing of original draft; All authors: writing, review and editing.

15
16 Acknowledgements. Thanks to the Chilean Weather Office for keeping up and running the Tololo station, particularly to
17 meteorologist Luis Valle. Technical support from engineer Sebastian Villalón is acknowledged. The first author made limited
18 use of <https://researchassistant.nature.com/> to improve the clarity of the text. Maria Kanakidou gratefully acknowledges the
19 support received from the U Bremen Excellence Chair Program. We are very grateful for the provision and maintenance of
20 CO and CH₄ measurements and data at Tololo by the Chilean Weather Office (DMC) and Mr. Gastón Torres, and the Swiss
21 Federal Laboratories for Materials Science and Technology (EMPA) and Dr. Martin Steinbacher. We are sorry for not having
22 invited Dr. Steinbacher to be a co-author but at the time we noticed this error, the paper was already written.

23
24 Financial support. Chilean researchers received support from FONDAP/ANID 1523A0002. The atmospheric chemistry
25 simulations were partly performed on the HPC cluster *Aether* at the University of Bremen, financed by the Deutsche
26 Forschungsgemeinschaft (DFG, German Research Foundation) under Germany's Excellence Strategy (University Allowance,
27 EXC 2077, University of Bremen).

1 **References**

2 Ainsworth, E. A.: Understanding and improving global crop response to ozone pollution, *Plant Journal*, 90, 886–897,
3 <https://doi.org/10.1111/tpj.13298>, 2017.

4 Akritidis, D., Pozzer, A., and Zanis, P.: On the impact of future climate change on tropopause folds and tropospheric
5 ozone, *Atmos. Chem. Phys.*, 19, 14387–14401, <https://doi.org/10.5194/acp-19-14387-2019>, 2019.

6 Anet, G. J., Steinbacher, M., Gallardo, L., Velásquez Álvarez, A. P., Emmenegger, L., and Buchmann, B.: Surface
7 ozone in the Southern Hemisphere: 20 years of data from a site with a unique setting in El Tololo, Chile, *Atmos. Chem. Phys.*,
8 17, 6477–6492, <https://doi.org/10.5194/acp-17-6477-2017>, 2017.

9 Barrett, B. S., Fitzmaurice, S. J., and Pritchard, S. R.: Intraseasonal variability of surface ozone in Santiago, Chile:
10 Modulation by phase of the Madden-Julian Oscillation (MJO), *Atmos. Environ.*, 57, 55–62,
11 <https://doi.org/10.1016/j.atmosenv.2012.04.040>, 2012.

12 Bourgeois, I., Peischl, J., Neuman, J. A., Brown, S. S., Thompson, C. R., Aikin, K. C., Allen, H. M., Angot, H., Apel,
13 E. C., Baublitz, C. B., Brewer, J. F., Campuzano-Jost, P., Commane, R., Crouse, J. D., Daube, B. C., DiGangi, J. P., Diskin,
14 G. S., Emmons, L. K., Fiore, A. M., Gkatzelis, G. I., Hills, A., Hornbrook, R. S., Huey, L. G., Jimenez, J. L., Kim, M., Lacey,
15 F., McKain, K., Murray, L. T., Nault, B. A., Parrish, D. D., Ray, E., Sweeney, C., Tanner, D., Wofsy, S. C., and Ryerson, T.
16 B.: Large contribution of biomass burning emissions to ozone throughout the global remote troposphere, *Proceedings of the*
17 *National Academy of Sciences*, 118, <https://doi.org/10.1073/pnas.2109628118>, 2021.

18 Bozkurt, D., Rojas, M., Boisier, J. P., Rondanelli, R., Garreaud, R., and Gallardo, L.: Dynamical downscaling over
19 the complex terrain of southwest South America: present climate conditions and added value analysis, *Clim. Dyn.*, 53, 6745–
20 6767, <https://doi.org/10.1007/s00382-019-04959-y>, 2019.

21 Cannon, A. J., Sobie, S. R., and Murdock, T. Q.: Bias Correction of GCM Precipitation by Quantile Mapping: How
22 Well Do Methods Preserve Changes in Quantiles and Extremes?, *J. Clim.*, 28, 6938–6959, [https://doi.org/10.1175/JCLI-D-](https://doi.org/10.1175/JCLI-D-14-00754.1)
23 14-00754.1, 2015.

24 Capparelli, V., Franzke, C., Vecchio, A., Freeman, M. P., Watkins, N. W., and Carbone, V.: A spatiotemporal analysis
25 of U.S. station temperature trends over the last century, *Journal of Geophysical Research Atmospheres*, 118, 7427–7434,
26 <https://doi.org/10.1002/jgrd.50551>, 2013.

27 Carrasco-Escaff, T., Garreaud, R., Bozkurt, D., Jacques-Coper, M., and Pauchard, A.: The key role of extreme
28 weather and climate change in the occurrence of exceptional fire seasons in south-central Chile, *Weather Clim. Extrem.*, 45,
29 100716, <https://doi.org/10.1016/j.wace.2024.100716>, 2024.

30 Chang, K. L., Schultz, M. G., Lan, X., McClure-Begley, A., Petropavlovskikh, I., Xu, X., and Ziemke, J. R.: Trend
31 detection of atmospheric time series: Incorporating appropriate uncertainty estimates and handling extreme events,
32 <https://doi.org/10.1525/elementa.2021.00035>, 15 December 2021.

33 Chang, K.-L., Schultz, M. G., Koren, G., and Selke, N.: Guidance note on best statistical practices for TOAR analyses,
34 2023.

1 Checa-Garcia, R., Hegglin, M. I., Kinnison, D., Plummer, D. A., and Shine, K. P.: Historical Tropospheric and
2 Stratospheric Ozone Radiative Forcing Using the CMIP6 Database, *Geophys. Res. Lett.*, 45, 3264–3273,
3 <https://doi.org/10.1002/2017GL076770>, 2018.

4 Christiansen, A., Mickley, L. J., Liu, J., Oman, L. D., and Hu, L.: Multidecadal increases in global tropospheric ozone
5 derived from ozonesonde and surface site observations: Can models reproduce ozone trends?, *Atmos. Chem. Phys.*, 22, 14751–
6 14782, <https://doi.org/10.5194/acp-22-14751-2022>, 2022.

7 Clifton, O. E., Fiore, A. M., Massman, W. J., Baublitz, C. B., Coyle, M., Emberson, L., Fares, S., Farmer, D. K.,
8 Gentine, P., Gerosa, G., Guenther, A. B., Helmig, D., Lombardozzi, D. L., Munger, J. W., Patton, E. G., Pusede, S. E.,
9 Schwede, D. B., Silva, S. J., Sörgel, M., Steiner, A. L., and Tai, A. P. K.: Dry Deposition of Ozone Over Land: Processes,
10 Measurement, and Modeling, <https://doi.org/10.1029/2019RG000670>, 1 March 2020.

11 Cooper, O. R., Parrish, D. D., Ziemke, J., Balashov, N. V., Cupeiro, M., Galbally, I. E., Gilge, S., Horowitz, L.,
12 Jensen, N. R., Lamarque, J. F., Naik, V., Oltmans, S. J., Schwab, J., Shindell, D. T., Thompson, A. M., Thouret, V., Wang, Y.,
13 and Zbinden, R. M.: Global distribution and trends of tropospheric ozone: An observation-based review, *Elementa*, 2,
14 <https://doi.org/10.12952/journal.elementa.000029>, 2014.

15 Cooper, O. R., Schultz, M. G., Schroeder, S., Chang, K.-L., Gaudel, A., Benítez, G. C., Cuevas, E., Fröhlich, M.,
16 Galbally, I. E., Molloy, S., Kubistin, D., Lu, X., McClure-Begley, A., Nédélec, P., O'Brien, J., Oltmans, S. J.,
17 Petropavlovskikh, I., Ries, L., Senik, I., Sjöberg, K., Solberg, S., Spain, G. T., Spangl, W., Steinbacher, M., Tarasick, D.,
18 Thouret, V., and Xu, X.: Multi-decadal surface ozone trends at globally distributed remote locations, *Elementa: Science of the*
19 *Anthropocene*, 8, 23, <https://doi.org/10.1525/elementa.420>, 2020.

20 Crutzen, P. J.: Tropospheric Ozone: An Overview, in: *Tropospheric Ozone*, Springer Netherlands, Dordrecht, 3–32,
21 https://doi.org/10.1007/978-94-009-2913-5_1, 1988.

22 Crutzen, P. J., Lawrence, M. G., and Pöschl, U.: On the background photochemistry of tropospheric ozone, *Tellus B:*
23 *Chemical and Physical Meteorology*, 51, 123, <https://doi.org/10.3402/tellusb.v51i1.16264>, 1999.

24 Cui, J., Sprenger, M., Staehelin, J., Siegrist, A., Kunz, M., Henne, S., and Steinbacher, M.: Impact of stratospheric
25 intrusions and intercontinental transport on ozone at Jungfrauoch in 2005: Comparison and validation of two Lagrangian
26 approaches, *Atmos. Chem. Phys.*, 9, 3371–3383, <https://doi.org/10.5194/acp-9-3371-2009>, 2009.

27 Daskalakis, N., Gallardo, L., Kanakidou, M., Nüß, J. R., Menares, C., Rondanelli, R., Thompson, A. M., and
28 Vrekoussis, M.: Impact of biomass burning and stratospheric intrusions in the remote South Pacific Ocean troposphere, *Atmos.*
29 *Chem. Phys.*, 22, 4075–4099, <https://doi.org/10.5194/acp-22-4075-2022>, 2022.

30 East, J. D., Jacob, D. J., Balasus, N., Bloom, A. A., Bruhwiler, L., Chen, Z., Kaplan, J. O., Mickley, L. J., Mooring,
31 T. A., Penn, E., Poulter, B., Sulprizio, M. P., Worden, J. R., Yantosca, R. M., and Zhang, Z.: Interpreting the Seasonality of
32 Atmospheric Methane, *Geophys. Res. Lett.*, 51, [Fiore https://doi.org/10.1029/2024GL108494](https://doi.org/10.1029/2024GL108494), 2024.

1 [Fiore, A. M., J. J. West, L. W. Horowitz, V. Naik, and M. D. Schwarzkopf \(2008\). Characterizing the tropospheric](#)
2 [ozone response to methane emission controls and the benefits to climate and air quality, *J. Geophys. Res.*, 113, D08307,](#)
3 [doi:10.1029/2007JD009162.](#)

4 Fleming, Z. L., Doherty, R. M., Von Schneidmesser, E., Malley, C. S., Cooper, O. R., Pinto, J. P., Colette, A., Xu,
5 X., Simpson, D., Schultz, M. G., Lefohn, A. S., Hamad, S., Moolla, R., Solberg, S., and Feng, Z.: Tropospheric Ozone
6 Assessment Report: Present-day ozone distribution and trends relevant to human health, *Elementa*, 6, 12,
7 <https://doi.org/10.1525/elementa.273>, 2018.

8 Forster, P., T. S. K. A. W. C. J.-L. D. D. F. D. J. L. T. M. M. D. P. M. W. M. W. and H. Z.: The Earth's Energy
9 Budget, Climate Feedbacks and Climate Sensitivity, in: *Climate Change 2021 – The Physical Science Basis*, Cambridge
10 University Press, 923–1054, <https://doi.org/10.1017/9781009157896.009>, 2021.

11 Franzke, C.: Nonlinear trends, long-range dependence, and climate noise properties of surface temperature, *J. Clim.*,
12 25, 4172–4183, <https://doi.org/10.1175/JCLI-D-11-00293.1>, 2012.

13 Fu, B., Gasser, T., Li, B., Tao, S., Ciaï, P., Piao, S., Balkanski, Y., Li, W., Yin, T., Han, L., Li, X., Han, Y., An, J.,
14 Peng, S., and Xu, J.: Short-lived climate forcings have long-term climate impacts via the carbon–climate feedback, *Nat. Clim.*
15 *Chang.*, 10, 851–855, <https://doi.org/10.1038/s41558-020-0841-x>, 2020.

16 Fuenzalida, H. A., Sánchez, R., and Garreaud, R. D.: A climatology of cutoff lows in the Southern Hemisphere,
17 *Journal of Geophysical Research D: Atmospheres*, 110, 1–10, <https://doi.org/10.1029/2005JD005934>, 2005.

18 Gallardo, L., Carrasco, J., and Olivares, G.: An analysis of ozone measurements at Cerro Tololo (30°S, 70°W, 2200
19 m.a.s.l.) in Chile, *Tellus B Chem. Phys. Meteorol.*, 52, 50–59, <https://doi.org/10.3402/tellusb.v52i1.16081>, 2000.

20 Gallardo, L., Henríquez, A., Thompson, A. M., Rondanelli, R., Carrasco, J., Orfanos-Cheuquelaf, A., and Squez, P.
21 V.: The first twenty years (1994–2014) of ozone soundings from Rapa Nui (27°S, 109°W, 51m a.s.l.), *Tellus B Chem. Phys.*
22 *Meteorol.*, 68, 29484, <https://doi.org/10.3402/tellusb.v68.29484>, 2016.

23 Garreaud, R. D., Vuille, M., Compagnucci, R., and Marengo, J.: Present-day South American climate, *Palaeogeogr.*
24 *Palaeoclimatol. Palaeoecol.*, 281, 180–195, <https://doi.org/10.1016/j.palaeo.2007.10.032>, 2009.

25 Garreaud, R. D., Boisier, J. P., Rondanelli, R., Montecinos, A., Sepúlveda, H. H., and Veloso-Aguila, D.: The Central
26 Chile Mega Drought (2010–2018): A climate dynamics perspective, *International Journal of Climatology*, 40, 421–439,
27 <https://doi.org/10.1002/joc.6219>, 2020.

28 Gaudel, A., Cooper, O. R., Ancellet, G., Barret, B., Boynard, A., Burrows, J. P., Clerbaux, C., Coheur, P.-F., Cuesta,
29 J., Cuevas, E., Doniki, S., Dufour, G., Ebojje, F., Foret, G., Garcia, O., Granados-Muñoz, M. J., Hannigan, J. W., Hase, F.,
30 Hassler, B., Huang, G., Hurtmans, D., Jaffe, D., Jones, N., Kalabokas, P., Kerridge, B., Kulawik, S., Latter, B., Leblanc, T.,
31 Le Flochmoën, E., Lin, W., Liu, J., Liu, X., Mahieu, E., McClure-Begley, A., Neu, J. L., Osman, M., Palm, M., Petetin, H.,
32 Petropavlovskikh, I., Querel, R., Rapp, N., Rozanov, A., Schultz, M. G., Schwab, J., Siddans, R., Smale, D., Steinbacher,
33 M., Tanimoto, H., Tarasick, D. W., Thouret, V., Thompson, A. M., Trickl, T., Weatherhead, E., Wespes, C., Worden, H. M.,
34 Vigouroux, C., Xu, X., Zeng, G., and Ziemke, J.: Tropospheric Ozone Assessment Report: Present-day distribution and trends

1 of tropospheric ozone relevant to climate and global atmospheric chemistry model evaluation, *Elementa: Science of the*
2 *Anthropocene*, 6, <https://doi.org/10.1525/elementa.291>, 2018.

3 González, M. E., Gómez-González, S., Lara, A., Garreaud, R., and Díaz-Hormazábal, I.: The 2010–2015
4 Megadrought and its influence on the fire regime in central and south-central Chile, *Ecosphere*, 9,
5 <https://doi.org/10.1002/ecs2.2300>, 2018.

6 Griffiths, P. T., Murray, L. T., Zeng, G., Shin, Y. M., Abraham, N. L., Archibald, A. T., Deushi, M., Emmons, L. K.,
7 Galbally, I. E., Hassler, B., Horowitz, L. W., Keeble, J., Liu, J., Moeini, O., Naik, V., O’Connor, F. M., Oshima, N., Tarasick,
8 D., Tilmes, S., Turnock, S. T., Wild, O., Young, P. J., and Zanis, P.: Tropospheric ozone in CMIP6 simulations, *Atmos. Chem.*
9 *Phys.*, 21, 4187–4218, <https://doi.org/10.5194/acp-21-4187-2021>, 2021.

10 Gulev, S.K., P.W. Thorne, J. Ahn, F.J. Dentener, C.M. Domingues, S. Gerland, D. Gong, D.S. Kaufman, H.C.
11 Nnamchi, J. Quaas, J.A. Rivera, S. Sathyendranath, S.L. Smith, B. Trewin, K. von Schuckmann, and R.S. Vose: Changing
12 State of the Climate System, in: *Climate Change 2021 – The Physical Science Basis*, edited by: (IPCC), I. P. on C. C.,
13 Cambridge University Press, Cambridge, 287–422, <https://doi.org/10.1017/9781009157896.004>, 2023.

14 Hastie, T. and Tibshirani, R.: Generalized Additive Models, *Statistical Science*, 1,
15 <https://doi.org/10.1214/ss/1177013604>, 1986.

16 Hastie, T., Tibshirani, R., and Friedman, J.: Boosting and Additive Trees, 1–51, https://doi.org/10.1007/b94608_10,
17 2009.

18 He, J., Naik, V., Horowitz, L. W., Dlugokencky, E., and Thoning, K.: Investigation of the global methane budget
19 over 1980–2017 using GFDL-AM4.1, *Atmos. Chem. Phys.*, 20, 805–827, <https://doi.org/10.5194/acp-20-805-2020>, 2020.

20 Hersbach, H., Bell, B., Berrisford, P., Hirahara, S., Horányi, A., Muñoz-Sabater, J., Nicolas, J., Peubey, C., Radu, R.,
21 Schepers, D., Simmons, A., Soci, C., Abdalla, S., Abellan, X., Balsamo, G., Bechtold, P., Biavati, G., Bidlot, J., Bonavita, M.,
22 De Chiara, G., Dahlgren, P., Dee, D., Diamantakis, M., Dragani, R., Flemming, J., Forbes, R., Fuentes, M., Geer, A.,
23 Haimberger, L., Healy, S., Hogan, R. J., Hólm, E., Janisková, M., Keeley, S., Laloyaux, P., Lopez, P., Lupu, C., Radnoti, G.,
24 de Rosnay, P., Rozum, I., Vamborg, F., Villaume, S., and Thépaut, J.: The ERA5 global reanalysis, *Quarterly Journal of the*
25 *Royal Meteorological Society*, 146, 1999–2049, <https://doi.org/10.1002/qj.3803>, 2020.

26 Hoesly, R. M., Smith, S. J., Feng, L., Klimont, Z., Janssens-Maenhout, G., Pitkanen, T., Seibert, J. J., Vu, L., Andres,
27 R. J., Bolt, R. M., Bond, T. C., Dawidowski, L., Kholod, N., Kurokawa, J. I., Li, M., Liu, L., Lu, Z., Moura, M. C. P., O’Rourke,
28 P. R., and Zhang, Q.: Historical (1750–2014) anthropogenic emissions of reactive gases and aerosols from the Community
29 Emissions Data System (CEDS), *Geosci. Model Dev.*, 11, 369–408, <https://doi.org/10.5194/gmd-11-369-2018>, 2018.

30 [Holton, J. R.: On the Global Exchange of Mass between the Stratosphere and Troposphere. *J. Atmos Sci*, 392–395,](https://doi.org/https://doi.org/10.1175/1520-0469(1990)047%3C0392:OTGEOM%3E2.0.CO;2)
31 [https://doi.org/https://doi.org/10.1175/1520-0469\(1990\)047%3C0392:OTGEOM%3E2.0.CO;2](https://doi.org/https://doi.org/10.1175/1520-0469(1990)047%3C0392:OTGEOM%3E2.0.CO;2), 1990.

32 Hu, Y., Huang, H., and Zhou, C.: Widening and weakening of the Hadley circulation under global warming, *Sci.*
33 *Bull. (Beijing)*, 63, 640–644, <https://doi.org/10.1016/j.scib.2018.04.020>, 2018.

1 [Inness, A., Benedetti, A., Flemming, J., Huijnen, V., Kaiser, J. W., Parrington, M., and Remy, S.: The ENSO signal](#)
2 [in atmospheric composition fields: emission-driven versus dynamically induced changes, *Atmos. Chem. Phys.*, 15, 9083–](#)
3 [9097, <https://doi.org/10.5194/acp-15-9083-2015>, 2015.](#)

4 Jacob, D. J. and Winner, D. A.: Effect of climate change on air quality, *Atmos. Environ.*, 43, 51–63,
5 <https://doi.org/10.1016/j.atmosenv.2008.09.051>, 2009.

6 Kalthoff, N., Bischoff-Gauß, I., Fiebig-Wittmaack, M., Fiedler, F., Thürauf, J., Novoa, E., Pizarro, C., Castillo, R.,
7 Gallardo, L., Rondanelli, R., and Kohler, M.: Mesoscale wind regimes in Chile at 30°S, *Journal of Applied Meteorology*, 41,
8 953–970, [https://doi.org/10.1175/1520-0450\(2002\)041<0953:MWRICA>2.0.CO;2](https://doi.org/10.1175/1520-0450(2002)041<0953:MWRICA>2.0.CO;2), 2002.

9 Kovács, L.: Feature selection algorithms in generalized additive models under concurrency, *Comput. Stat.*, 39, 461–
10 493, <https://doi.org/10.1007/s00180-022-01292-7>, 2024.

11 Kuai, L., Bowman, K. W., Worden, H. M., Herman, R. L., and Kulawik, S. S.: Hydrological controls on the
12 tropospheric ozone greenhouse gas effect, *Elementa: Science of the Anthropocene*, 5, <https://doi.org/10.1525/elementa.208>,
13 2017.

14 Kumar Mishra, A., Sen Gupta, G., Abha Singh, A., Bhushan Agrawal, S., and Tiwari, S.: Can fertilization OF CO2
15 heal the ozone-injured agroecosystems?, *Atmos. Pollut. Res.*, 15, 102046, <https://doi.org/10.1016/j.apr.2024.102046>, 2024.

16 Lapere, R., Mailler, S., and Menut, L.: The 2017 Mega-Fires in Central Chile: Impacts on Regional Atmospheric
17 Composition and Meteorology Assessed from Satellite Data and Chemistry-Transport Modeling, *Atmosphere (Basel)*, 12,
18 344, <https://doi.org/10.3390/atmos12030344>, 2021.

19 Li, Y., Xia, Y., Xie, F., and Yan, Y.: Influence of stratosphere-troposphere exchange on long-term trends of surface
20 ozone in CMIP6, *Atmos. Res.*, 297, 107086, <https://doi.org/10.1016/j.atmosres.2023.107086>, 2024.

21 Lipovetsky, S. and Conklin, M.: Analysis of regression in game theory approach, *Appl. Stoch. Models Bus. Ind.*, 17,
22 319–330, <https://doi.org/10.1002/asmb.446>, 2001.

23 Lu, X., Zhang, L., Zhao, Y., Jacob, D. J., Hu, Y., Hu, L., Gao, M., Liu, X., Petropavlovskikh, I., McClure-Begley,
24 A., and Querel, R.: Surface and tropospheric ozone trends in the Southern Hemisphere since 1990: possible linkages to
25 poleward expansion of the Hadley circulation, *Sci. Bull. (Beijing)*, 64, 400–409, <https://doi.org/10.1016/j.scib.2018.12.021>,
26 2019.

27 [Matus, F., Rondanelli, R., Rutllant, J., & Henderson, S. \(2025\). Mechanisms for the influence of the MJO on](#)
28 [precipitation in Southwestern South America. *Journal of Geophysical Research: Atmospheres*, 130,](#)
29 [e2024JD041935. <https://doi.org/10.1029/2024JD041935>](#)

30 Van Marle, M. J. E., Kloster, S., Magi, B. I., Marlon, J. R., Daniau, A. L., Field, R. D., Arneth, A., Forrest, M.,
31 Hantson, S., Kehrwald, N. M., Knorr, W., Lasslop, G., Li, F., Mangeon, S., Yue, C., Kaiser, J. W., and Van Der Werf, G. R.:
32 Historic global biomass burning emissions for CMIP6 (BB4CMIP) based on merging satellite observations with proxies and
33 fire models (1750–2015), <https://doi.org/10.5194/gmd-10-3329-2017>, 11 September 2017.

1 Mills, G., Harmens, H., Wagg, S., Sharps, K., Hayes, F., Fowler, D., Sutton, M., and Davies, B.: Ozone impacts on
2 vegetation in a nitrogen enriched and changing climate, *Environmental Pollution*, 208, 898–908,
3 <https://doi.org/10.1016/j.envpol.2015.09.038>, 2016.

4 Molnar, C.: *Interpretable Machine Learning. A Guide for Making Black Box Models Explainable.*, Third Edition.,
5 247 pp., 2025.

6 Muggeo, V. M. R.: Interval estimation for the breakpoint in segmented regression: a smoothed score-based approach,
7 *Aust. N. Z. J. Stat.*, 59, 311–322, <https://doi.org/10.1111/anzs.12200>, 2017.

8 Murray, L. T., Mickley, L. J., Kaplan, J. O., Sofen, E. D., Pfeiffer, M., and Alexander, B.: Factors controlling
9 variability in the oxidative capacity of the troposphere since the Last Glacial Maximum, *Atmos. Chem. Phys.*, 14, 3589–3622,
10 <https://doi.org/10.5194/acp-14-3589-2014>, 2014.

11 Myhre, G., Shindell, D., Bréon, F.-M., Collins, W., Fuglestedt, J., Huang, J., Koch, D., Lamarque, J.-F., Lee, D.,
12 Mendoza, B., Nakajima, T., Robock, A., Stephens, G., Takemura, T., and Zhang, H.: Anthropogenic and Natural Radiative
13 Forcing, in: *Climate Change 2013: The Physical Science Basis. Contribution of Working Group I to the Fifth Assessment*
14 *Report of the Intergovernmental Panel on Climate Change*, edited by: Stocker, T. F., Qin, D., Plattner, G.-K., Tignor, M.,
15 Allen, S. K., Boschung, J., Nauels, A., Xia, Y., Bex, V., and Midgley, P. M., Cambridge University Press, 659–740,
16 <https://doi.org/10.1017/CBO9781107415324.018>, 2013.

17 [Neu, J. L., Flury, T., Manney, G. L., Santee, M. L., Livesey, N. J., & Worden, J. \(2014\). Tropospheric ozone variations](#)
18 [governed by changes in stratospheric circulation. *Nature Geoscience*, 7\(5\), 340–344. <https://doi.org/10.1038/ngeo2138>](#)

19 Nisbet, E. G., Manning, M. R., Dlugokencky, E. J., Fisher, R. E., Lowry, D., Michel, S. E., Myhre, C. L., Platt, S. M.,
20 Allen, G., Bousquet, P., Brownlow, R., Cain, M., France, J. L., Hermansen, O., Hossaini, R., Jones, A. E., Levin, I., Manning,
21 A. C., Myhre, G., Pyle, J. A., Vaughn, B. H., Warwick, N. J., and White, J. W. C.: Very Strong Atmospheric Methane Growth
22 in the 4 Years 2014–2017: Implications for the Paris Agreement, *Global Biogeochem. Cycles*, 33, 318–342,
23 <https://doi.org/10.1029/2018GB006009>, 2019.

24 Nuvolone, D., Petri, D., and Voller, F.: The effects of ozone on human health, *Environmental Science and Pollution*
25 *Research*, 25, 8074–8088, <https://doi.org/10.1007/s11356-017-9239-3>, 2018.

26 Porter, W. C. and Heald, C. L.: The mechanisms and meteorological drivers of the summertime ozone-temperature
27 relationship, *Atmos. Chem. Phys.*, 19, 13367–13381, <https://doi.org/10.5194/acp-19-13367-2019>, 2019.

28 Pusede, S. E., Steiner, A. L., and Cohen, R. C.: Temperature and Recent Trends in the Chemistry of Continental
29 Surface Ozone, <https://doi.org/10.1021/cr5006815>, 27 May 2015.

30 Rondanelli, R.: Cutoff Lows Over Southwestern South America, in: *Oxford Research Encyclopedia of Climate*
31 *Science*, Oxford University Press, Oxford, <https://doi.org/10.1093/acrefore/9780190228620.013.976>, 2025.

32 Rondanelli, R., Gallardo, L., and Garreaud, R. D.: Rapid changes in ozone mixing ratios at Cerro Tololo (30°10'S,
33 70°48'W, 2200 m) in connection with cutoff lows and deep troughs, *Journal of Geophysical Research Atmospheres*, 107, ACL
34 6-1-ACL 6-15, <https://doi.org/10.1029/2001JD001334>, 2002.

1 Rowlinson, M. J., Rap, A., Arnold, S. R., Pope, R. J., Chipperfield, M. P., McNorton, J., Forster, P., Gordon, H.,
2 Pringle, K. J., Feng, W., Kerridge, B. J., Latter, B. L., and Siddans, R.: Impact of El Niño–Southern Oscillation on the
3 interannual variability of methane and tropospheric ozone, *Atmos. Chem. Phys.*, 19, 8669–8686, [https://doi.org/10.5194/acp-](https://doi.org/10.5194/acp-19-8669-2019)
4 [19-8669-2019](https://doi.org/10.5194/acp-19-8669-2019), 2019.

5 Saunio, M., Stavert, A. R., Poulter, B., Bousquet, P., Canadell, J. G., Jackson, R. B., Raymond, P. A., Dlugokencky,
6 E. J., Houweling, S., Patra, P. K., Ciais, P., Arora, V. K., Bastviken, D., Bergamaschi, P., Blake, D. R., Brailsford, G.,
7 Bruhwiler, L., Carlson, K. M., Carrol, M., Castaldi, S., Chandra, N., Crevoisier, C., Crill, P. M., Covey, K., Curry, C. L.,
8 Etiope, G., Frankenberg, C., Gedney, N., Hegglin, M. I., Höglund-Isaksson, L., Hugelius, G., Ishizawa, M., Ito, A., Janssens-
9 Maenhout, G., Jensen, K. M., Joos, F., Kleinen, T., Krummel, P. B., Langenfelds, R. L., Laruelle, G. G., Liu, L., Machida, T.,
10 Maksyutov, S., McDonald, K. C., McNorton, J., Miller, P. A., Melton, J. R., Morino, I., Müller, J., Murguia-Flores, F., Naik,
11 V., Niwa, Y., Noce, S., O’Doherty, S., Parker, R. J., Peng, C., Peng, S., Peters, G. P., Prigent, C., Prinn, R., Ramonet, M.,
12 Regnier, P., Riley, W. J., Rosentreter, J. A., Segers, A., Simpson, I. J., Shi, H., Smith, S. J., Steele, L. P., Thornton, B. F., Tian,
13 H., Tohjima, Y., Tubiello, F. N., Tsuruta, A., Viovy, N., Voulgarakis, A., Weber, T. S., van Weele, M., van der Werf, G. R.,
14 Weiss, R. F., Worthy, D., Wunch, D., Yin, Y., Yoshida, Y., Zhang, W., Zhang, Z., Zhao, Y., Zheng, B., Zhu, Q., Zhu, Q., and
15 Zhuang, Q.: The Global Methane Budget 2000–2017, *Earth Syst. Sci. Data*, 12, 1561–1623, [https://doi.org/10.5194/essd-12-](https://doi.org/10.5194/essd-12-1561-2020)
16 [1561-2020](https://doi.org/10.5194/essd-12-1561-2020), 2020.

17 Schwertfeger, B. T., Lohmann, G., and Lipskoch, H.: Introduction of the BiasAdjustCXX command-line tool for the
18 application of fast and efficient bias corrections in climatic research, *SoftwareX*, 22,
19 <https://doi.org/10.1016/j.softx.2023.101379>, 2023.

20 Seguel, R. J., Morales S., R. G. E., and Leiva G., M. A.: Ozone weekend effect in Santiago, Chile, *Environmental*
21 *Pollution*, 162, 72–79, <https://doi.org/10.1016/j.envpol.2011.10.019>, 2012.

22 Seguel, R. J., Castillo, L., Opazo, C., Rojas, N. Y., Nogueira, T., Cazorla, M., Gavidia-Calderón, M., Gallardo, L.,
23 Garreaud, R., Carrasco-Escaff, T., and Elshorbany, Y.: Changes in South American surface ozone trends: exploring the
24 influences of precursors and extreme events, *Atmos. Chem. Phys.*, 24, 8225–8242, <https://doi.org/10.5194/acp-24-8225-2024>,
25 2024.

26 Sekiya, T. and Sudo, K.: Role of meteorological variability in global tropospheric ozone during 1970–2008, *Journal*
27 *of Geophysical Research: Atmospheres*, 117, <https://doi.org/10.1029/2012JD018054>, 2012.

28 Skeie, R. B., Myhre, G., Hodnebrog, Ø., Cameron-Smith, P. J., Deushi, M., Hegglin, M. I., Horowitz, L. W., Kramer,
29 R. J., Michou, M., Mills, M. J., Olivie, D. J. L., Connor, F. M. O., Paynter, D., Samset, B. H., Sellar, A., Shindell, D., Takemura,
30 T., Tilmes, S., and Wu, T.: Historical total ozone radiative forcing derived from CMIP6 simulations, *NPJ Clim. Atmos. Sci.*,
31 3, <https://doi.org/10.1038/s41612-020-00131-0>, 2020.

32 Škerlak, B., Sprenger, M., and Wernli, H.: A global climatology of stratosphere-troposphere exchange using the ERA-
33 Interim data set from 1979 to 2011, *Atmos. Chem. Phys.*, 14, 913–937, <https://doi.org/10.5194/acp-14-913-2014>, 2014.

1 Snyder, C. W., Mastrandrea, M. D., and Schneider, S. H.: The Complex Dynamics of the Climate System: Constraints
2 on our Knowledge, Policy Implications and the Necessity of Systems Thinking, in: Philosophy of complex systems, Elsevier,
3 467–505, 2011.

4 Staehle, C., Rieder, H. E., Fiore, A. M., and Schnell, J. L.: Technical note: An assessment of the performance of
5 statistical bias correction techniques for global chemistry–climate model surface ozone fields, *Atmos. Chem. Phys.*, 24, 5953–
6 5969, <https://doi.org/10.5194/acp-24-5953-2024>, 2024.

7 Szopa, S., V. N. B. A. P. A. T. B. W. D. C. S. F. L. G. A. K.-S. Z. K. H. L. N. U. and P. Z.: Short-lived Climate
8 Forcers, in: *Climate Change 2021 – The Physical Science Basis*, edited by: Masson-Delmotte, V., P. Zhai, A. Pirani, S.L.
9 Connors, C. Péan, S. Berger, N. Caud, Y. Chen, L. Goldfarb, M. I. G. and M. Huang, K. Leitzell, E. Lonnoy, J.B.R. Matthews,
10 T.K. Maycock, T. Waterfield, O. Yelekçi, R. Yu, and B. Z., Cambridge University Press, United Kingdom and New York,
11 NY, USA, 817–922, <https://doi.org/10.1017/9781009157896.008>, 2021.

12 [David Tarasick, Ian E. Galbally, Owen R. Cooper, Martin G. Schultz, Gerard Ancellet, Thierry Leblanc, Timothy J.](#)
13 [Wallington, Jerry Ziemke, Xiong Liu, Martin Steinbacher, Johannes Staehelin, Corinne Vigouroux, James W. Hannigan,](#)
14 [Omaira García, Gilles Foret, Prodromos Zanis, Elizabeth Weatherhead, Irina Petropavlovskikh, Helen Worden, Mohammed](#)
15 [Osman, Jane Liu, Kai-Lan Chang, Audrey Gaudel, Meiyun Lin, Maria Granados-Muñoz, Anne M. Thompson, Samuel J.](#)
16 [Oltmans, Juan Cuesta, Gaëlle Dufour, Valerie Thouret, Birgit Hassler, Thomas Trickl, Jessica L. Neu; Tropospheric Ozone](#)
17 [Assessment Report: Tropospheric ozone from 1877 to 2016, observed levels, trends and uncertainties. *Elementa: Science of*](#)
18 [the Anthropocene](#) 1 January 2019; 7 39. doi: <https://doi.org/10.1525/elementa.376>

19 Thompson, A. M.: The oxidizing capacity of the Earth’s atmosphere: Probable past and future changes, *Science*
20 (1979)., 256, 1157–1165, <https://doi.org/10.1126/science.256.5060.1157>, 1992.

21 Thoning, K. W., Tans, P. P., and Komhyr, W. D.: Atmospheric carbon dioxide at Mauna Loa Observatory: 2. Analysis
22 of the NOAA GMCC data, 1974–1985, *Journal of Geophysical Research: Atmospheres*, 94, 8549–8565,
23 <https://doi.org/10.1029/JD094iD06p08549>, 1989.

24 Wang, S., Foster, A., Lenz, E. A., Kessler, J. D., Stroeve, J. C., Anderson, L. O., Turetsky, M., Betts, R., Zou, S., and
25 Liu, W.: Mechanisms and impacts of Earth system tipping elements, *Reviews of Geophysics*, 61, e2021RG000757, 2023.

26 Weatherhead, E. C., Reinsel, G. C., Tiao, G. C., Meng, X. L., Choi, D., Cheang, W. K., Keller, T., DeLuisi, J.,
27 Wuebbles, D. J., Kerr, J. B., Miller, A. J., Oltmans, S. J., and Frederick, J. E.: Factors affecting the detection of trends:
28 Statistical considerations and applications to environmental data, *Journal of Geophysical Research Atmospheres*, 103, 17149–
29 17161, <https://doi.org/10.1029/98JD00995>, 1998.

30 Weber, T., Wiseman, N. A., and Kock, A.: Global ocean methane emissions dominated by shallow coastal waters,
31 *Nat. Commun.*, 10, 4584, <https://doi.org/10.1038/s41467-019-12541-7>, 2019.

32 [West, J. J., A. M. Fiore, V. Naik, L. W. Horowitz, M. D. Schwarzkopf, and D. L. Mauzerall \(2008\), Ozone air quality](#)
33 [and radiative forcing consequences of changes in ozone precursor emissions, *Geophys. Res. Lett.*, 34, L06806,](#)
34 [doi:10.1029/2006GL029173](https://doi.org/10.1029/2006GL029173)

1 Yeung, L. Y., Murray, Lee. T., Martinerie, P., Witrant, E., Hu, H., Banerjee, A., Orsi, A., and Chappellaz, J.: Isotopic
2 constraint on the twentieth-century increase in tropospheric ozone, *Nature*, 570, 224–227, [https://doi.org/10.1038/s41586-019-](https://doi.org/10.1038/s41586-019-1277-1)
3 1277-1, 2019.

4 Young, P. J., Archibald, A. T., Bowman, K. W., Lamarque, J.-F., Naik, V., Stevenson, D. S., Tilmes, S., Voulgarakis,
5 A., Wild, O., Bergmann, D., Cameron-Smith, P., Cionni, I., Collins, W. J., Dalsøren, S. B., Doherty, R. M., Eyring, V.,
6 Faluvegi, G., Horowitz, L. W., Josse, B., Lee, Y. H., MacKenzie, I. A., Nagashima, T., Plummer, D. A., Righi, M., Rumbold,
7 S. T., Skeie, R. B., Shindell, D. T., Strode, S. A., Sudo, K., Szopa, S., and Zeng, G.: Pre-industrial to end 21st century
8 projections of tropospheric ozone from the Atmospheric Chemistry and Climate Model Intercomparison Project (ACCMIP),
9 *Atmos. Chem. Phys.*, 13, 2063–2090, <https://doi.org/10.5194/acp-13-2063-2013>, 2013.

10 Zhang, Y., Cooper, O. R., Gaudel, A., Thompson, A. M., Nédélec, P., Ogino, S. Y., and West, J. J.: Tropospheric
11 ozone change from 1980 to 2010 dominated by equatorward redistribution of emissions, *Nat. Geosci.*, 9, 875–879,
12 <https://doi.org/10.1038/ngeo2827>, 2016.

13 Zhang, Y., West, J. J., Emmons, L. K., Flemming, J., Jonson, J. E., Lund, M. T., Sekiya, T., Sudo, K., Gaudel, A.,
14 Chang, K., Nédélec, P., and Thouret, V.: Contributions of World Regions to the Global Tropospheric Ozone Burden Change
15 From 1980 to 2010, *Geophys. Res. Lett.*, 48, <https://doi.org/10.1029/2020GL089184>, 2021.

16

17